PTT-26

Some Properties of Mechanically Alloyed Oxide Dispersion Strengthened Metals

By

Adebayo Yekeen Badmos
Churchill College, Cambridge

Department of Materials Science and Metallurgy
Pembroke Street
Cambridge CB2 3QZ

A dissertation submitted for the degree of
Doctor of Philosophy
at the University of Cambridge
October 1997

PREFACE

This dissertation is submitted for the degree of Doctor of Philosophy at the University of Cambridge. The investigation described herein was carried out under the supervision of Dr. H. K. D. H. Bhadeshia in the Department of Materials Science and Metallurgy, University of Cambridge, between October 1994 and September 1997. Except where acknowledgement and reference to previous work is made, this work is, to the best of my knowledge, original and carried out without collaboration. Neither this , nor any similar dissertation has been or is being submitted for any degree, diploma or other qualification at any other University.

The contents of Chapters Four and Five have been accepted for publication and Chapter Six submitted for publication with the details as below.

(i) A. Y. Badmos and H. K. D. H. Bhadeshia (1997), "The Evolution of Solutions: A Thermodynamic Analysis of Mechanical Alloying' *Metallurgical Transactions A,* **28** 1–6.

(ii) A. Y. Badmos, H. K. D. H. Bhadeshia, and D.J.C. Mackay (1997), "Neural Network Models for the Tensile Properties of Mechanically Alloyed ODS Iron–Alloys" - Accepted for publication in *Materials Science and Technology.*

(iii) A. Y. Badmos and H. K. D. H. Bhadeshia (1997), "Yield Strength of Mechanically Alloyed ODS Iron Alloys : Physical Interpretation" - Submitted for publication in *Materials Science and Technology.*

Adebayo Yekeen Badmos

ACKNOWLEDGEMENTS

To Almighty God is due every praise and glory for the successful completion of this work. With gratitude I acknowledged the enormous financial commitments of my sponsors, Cambridge Commonwealth Trust for the Blue Circle Scholarship and the Committee of Vice–Chancellors and Principals of Universities, UK, for the Overseas Research Studentship (ORS).

I am particularly grateful to my supervisor, Dr. H. K. D. H. Bhadeshia without whose inspirational supervision, the timely completion of this work would not have been possible. His enthusiasm, patience, encouragement and seemingly inexhaustible pool of ideas have been found tremendously helpful in every aspect of this research. I wish to thank Professor Alan Windle for the provision of laboratory facilities in the Department of Materials Science and Metallurgy at the University of Cambridge. The help from the technical staff in the Department has been much appreciated, especially from Brian Whitmore, Brian Barber, Carol Best, Graham Morgan, Dave Nicol, Robinson Taylor and Kelvin Robert. I am also grateful to the entire members of my research group (Phase Transformation) for providing the friendly and stimulating working environment.

I would like to express my indebtedness to INCO Alloy, Hereford, UK, for the supply of the materials used in the experimental investigation of this work. Also, the intellectual contributions of the officers from the Research and Development Departments of INCO Alloy and National Power Plc. during the discussions at our series of meetings are acknowledged with thanks. I thank Dr. A.R. Jones, Liverpool University, UK., for providing some data for neural network analysis.

I warmly acknowledged the special position of my wife during the course of this work. Her moral support and encouragement were the sources of my emotional strength at those difficult times of the usual research frustration and low morale. Finally, I would like to say a big "THANK YOU" to my parents for their support and encouragement. This thesis is dedicated to them for all they went through for my education.

ABSTRACT

Oxide dispersion strengthened (ODS) superalloys are generally made using the mechanical alloying technique. In this, the powdered components are attrited together to form a solid solution with finely dispersed oxide particles. The material produced by compacting the powder using extrusion and rolling has exceptionally high creep resistance after a recrystallization heat–treatment. A great deal is understood about the microstructure but not the mechanical properties. The main purpose of this work was to model some of the mechanical properties of iron–base ODS alloys.

A brief introduction to the aim is followed by an extensive literature review dealing with all aspects of the process and the physical metallurgy of the resulting alloys. The experimental techniques used in the course of the investigations are described in Chapter Three.

The evolution of a solution during the attrition of mixtures of powders has been studied by developing a novel thermodynamic analysis which incorporates large particles rather than just atoms. Normal thermodynamic theory for solutions begins with the mixing of components atoms. However, in mechanical alloying, solutions are prepared by mixing together lumps of the components, each of which might contain millions of identical atoms. It has never been clear as to when the component powders become more like a solution than a mechanical mixture. It is predicted that solution formation by the mechanical alloying of solid components cannot occur unless there is a gain in coherency as the particles become small. The existence of a barrier to the evolution of solution due to interfacial energy is also identified.

The relationship between the tensile properties and a number of variables known to affect mechanical properties is studied using an artifitial neural network applied to the published data. Models have thus been produced dealing with the yield strength, ultimate tensile strength and elongation (Chapter Five). The analysis revealed patterns which are metallurgically significant and which permit

the quantitative estimation of mechanical properties as a function of important processing and service variables together with an indication of confidence limits.

The neural network models can express the output as a function of a very large number of interesting variables. An alternative approach involves modelling based on physical principles. The components of the yield strength of MA956, a mechanically alloyed ODS ferritic steel have been investigated quantitatively in Chapter Six. The ambient temperature yield strength of the alloy in the as–processed condition originates from its ultra–fine grain size, the intrinsic strength of ferritic iron, dispersoid strenthening via the yttria compounds and finally, the dislocation density. The contributions of these components decrease in the order stated. The contribution from dispersion strengthening has been estimated using dislocation theory and has been demonstrated to be consistent with that measured experimentally. It is found that much of the difference in strength between the recrystallised and unrecrystallised forms can be explained in terms of the grain structure.

Appendices I and II report the experimental investigations relating to the characteristic anisotropic mechanical behaviour of the alloys. Some tensile tests conducted to verify some of the results of the neural network analysis are reported in Appendix III.

CONTENTS

NOMENCLATURE AND ABBREVIATIONS

MA	Mechanical Alloying
ODS	Oxide Dispersion Strengthened
ΔG_f	Free energy of formation
γ'	Intermetallic phase in nickel–base alloys
F_r	Retarding force per unit area
f	Volume fraction of particles
r	Particle radius
γ_{gb}	Grain boundary energy per unit area
T	Temperature
T_m	Melting temperature
τ_{OR}	Orowan shear stress
f.c.c.	Face centered cubic
b.c.c.	Body centered cubic
σ_y	Yield strength
d	Grain size
σ_i	Lattice friction stress
k_o	Grain boundary locking parameter
τ_p	Resolved shear stress for dislocation by–pass
G	Shear modulus
b	Burgers vector
λ	Interparticle spacing
K',K'',K'''	Constants
H	Total hardness

H_m	Hardness due to matrix
K_p	Material constant for dispersed phase
GAR	Grain aspect ratio
σ_{eff}	Effective strength
σ_m	Inherent strength of ODS matrix
f_a	Volume average of dispersed particles
K	An interaction parameter for creep
δ_b	Gap between grain boundaries
σ_{Fe}	Strength of pure iron
σ_s	Solid solution strengthening
σ_p	Particle strengthening
σ_g	Grain boundary strengthening
σ_d	Dislocation strengthening
D_o	Pre-exponential component of self-diffusion coefficent
ρ	Dislocation density
$\dot{\epsilon}$	Shear strain rate
a_v	Area associated with a vacancy
k	Boltzmann constant
y	Output of neural network
x_j	Input of neural network
w_j	Weight of neural network
θ_i	Bias of neural network
h_i	Hyperbolic transfer function of neural network
x_N	Normalized value of input x_j
x_{min}	Minimum value of input x_j
x_{max}	Maximum value of input x_j

μ_A^o	Molar free energy of a pure component A
m_A	Atoms per powder particle of A
N_a	Avogadro number
ΔS_M	Entropy of mixing
ΔG_M	Free energy of mixing
ΔH_M	Enthalpy of mixing
ΔH_I	Change in energy due to interfaces
ϵ_{AA}	Binding energy between atoms of A

CHAPTER ONE

Introduction

1.1 Mechanically Alloyed ODS Superalloys

The need for materials with good high temperature capabilities has led to the development of the mechanical alloying (MA) technique for the production of oxide dispersion strengthened (ODS) superalloys. This includes both iron–base and nickel–base superalloys with fine and stable inert-oxide dispersions which improve the resistance to creep deformation. It is significant that with the MA process, the matrix composition and the nature of the dispersoids can be manipulated independently. The matrix composition can be tailored to optimize corrosion resistance and the dispersoids for strength. The nominal compositions of the commercially available mechanically alloyed oxide dispersion strengthened alloys are given in Table 1.1 and discussed in detail in Chapter Two.

Mechanical alloying involves the creation of an alloy by the intense mechanical deformation of mixtures of elemental or master–alloy powders. The powders are then consolidated by various powder metallurgical processes such as hot–isostatic pressing and extrusion. After mechanical alloying and consolidation, the alloys have a very fine grained microstructure and a very high hardness. A recrytallization heat–treatment is used to soften the alloy and to form a coarse columnar grain structure suitable for applications where creep resistance is important (Figure 1.1). The outstanding high temperature properties (about 1000 °C) of the alloys are therefore due to the uniform distribution of fine oxide particles, the coarse columnar grain structure, and the stable and adherent surface layer of protective oxide. Figure 1.2 illustrates a common method of manufacture for engineering applications.

Table 1.1 : Chemical compositions (wt.%) of some typical commercial MA–ODS alloys.

Steels	C	Cr	Al	Mo	Ti	N	Ti_2O_3	Y_2O_3	Fe
MA957	0.01	14.0	–	0.3	1.0	0.012	–	0.27	Balance
DT2203Y05		13.0	–	1.5	2.2		–	0.5	Balance
ODM 331		13.0	3.0	1.5	0.6		–	0.5	Balance
ODM 751		16.5	4.5	1.5	0.6		–	0.5	Balance
ODM 061		20.0	6.0	1.5	0.6		–	0.5	Balance
MA956	0.01	20.0	4.5	–	0.5	0.045	–	0.50	Balance
PM2000	< 0.04	20.0	5.5		0.5		–	0.5	Balance
PM2010	< 0.04	20.0	5.5		0.5		–	1.0	Balance
DT(DT2906)		13.0	–	1.5	2.9		1.8	–	Balance
DY(DT2203Y03)		13.0	–	1.5	2.2		0.9	0.5	Balance

Ni–Base	C	Cr	Al	Ti	W	Fe	N	Total O	Y_2O_3	Ni
MA754	0.05	20.0	0.3	0.5	–	–	–	0.37	0.6	Balance
MA6000	0.06	15.0	4.5	2.3	3.9	1.5	0.2	0.57	1.1	Balance
MA760	0.06	19.5	6.0	–	3.4	1.2	0.3	0.6	1.0	Balance
MA758	0.05	30.0	0.3	–	0.5	–	–	0.37	0.6	Balance

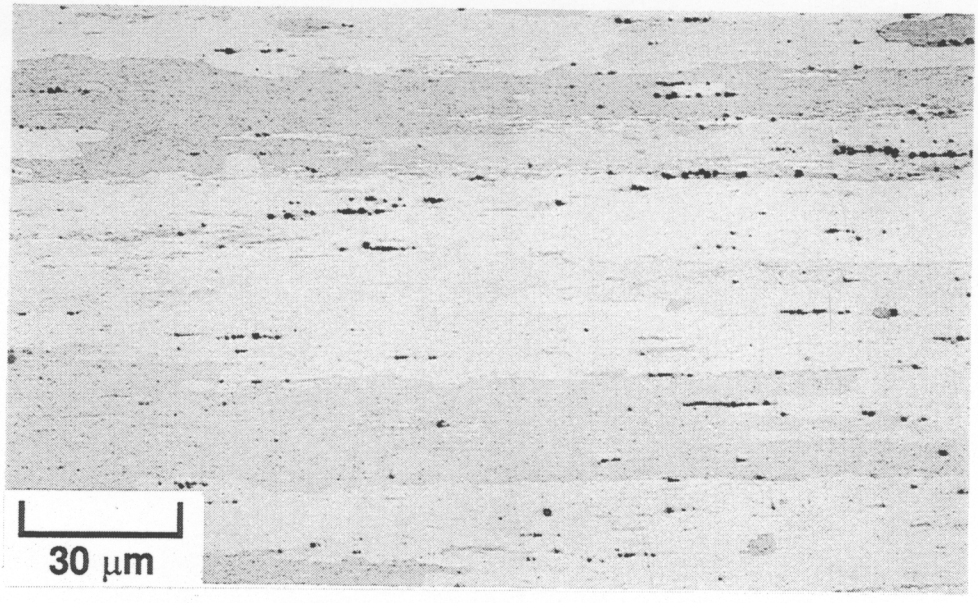

Figure 1.1: Typical microstructure of the mechanically alloyed ODS metal, MA956, after a recrystallization heat–treatment. The extrusion is horizontal in this micrograph.

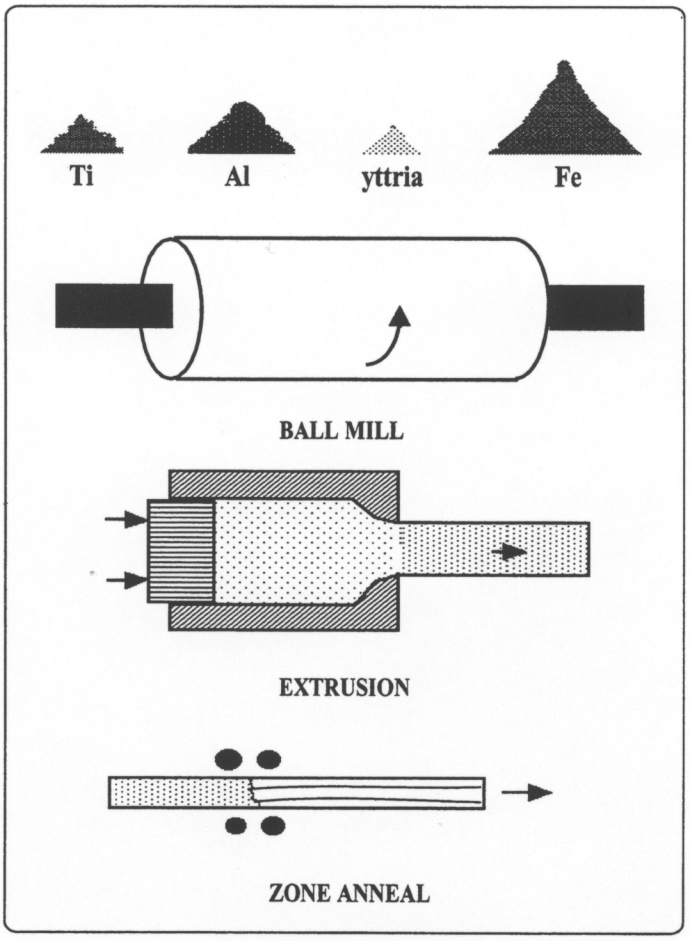

Figure 1.2 : Schematic illustration of the manufacturing process for mechanically alloyed metals.

1.2 Aims and objectives

Although, mechanically alloyed oxide dispersion stenghtened alloys are already available in commercial quantities, the technique is nevertheless special and a large number of important phenomena are not yet understood. Previous work has focussed on the control of microstructure but there has been no work on the way in which a solution evolves during the mechanical alloying process, nor on the modelling of mechanical properties. The evolution of the solid solution during the MA process is not understood even from a thermodynamic view point. Experimental measurements of the mechanical properties of the alloys are not yet exhaustive and the published data have not been properly coordinated to provide a definite pattern with regard to the numerous variables known to be important in understanding the service behaviour of the alloys. The columnar grain structure produced by directional recrystallisation is ideal for elevated temperature applications where creep resistance along the longitudinal direction is important. It is, however, less resistant to transverse stresses, which is a major disadvantage for tubular forms of the kind typical in heat exchangers. It is necessary therefore to understand the anisotropy inherent in the commercially available mechanically alloyed metals. The main objective of this work was to attempt to create quantitative models for some properties of these alloys.

CHAPTER TWO

Literature Review

2.1 Oxide Dispersion Strengthened (ODS) Alloys

When fine second phase particles are distributed in a crystalline matrix, a microstructure is formed which can be much stronger than the matrix phase alone. Such alloys are termed dispersion-strengthened materials [Ansell, 1966]. Oxides make the best dispersoids because of their high hardness, stability at high temperatures, inertness or insolubility in the matrix metals, and availability in fine particulate form. Oxides of reactive elements such as aluminium, silicon, beryllium, magnesium thorium, zirconium, and yttrium are preferable, because they are more stable at high temperatures than oxides of the more noble metals such as copper and nickel, which are suitable as matrix metals. There are many ways of adding oxide particles to metals.

The simple mechanical mixing technique involves the use of a high speed blender [Gregory and Goetzel, 1958; Zwilsky and Grant, 1962] or a ball mill [Tracey and Worn, 1962] to coat the surface of metallic powders with oxide. The interparticle spacing in the consolidated alloy produced from these powders is limited by the starting powder particle size. Powder sizes of less than 5 nm are required to get sufficiently fine interparticle spacings even with large mechanical reductions during consolidation and subsequent working operations. Powders this fine containing γ' (Ni_3[Al, Ti]) formers such as Al and Ti are very reactive because of their high specific surface area and complete or nearly complete oxidation of Al and Ti can result [Benjamin, 1970].

Ignition coating involves mixing alloy powders with a liquid solution of a salt of a reactive metal.

This mixture is dried and pulverized and the powders are heated in an inert or reducing environment to convert the salt into a refractory oxide [Murphy and Grant, 1962]. This technique also produces oxide coated powders which therefore have the same disadvantages as powders produced by the simple mechanical mixing technique. There is a greater degree of contamination because of the oxidizing potential of the reaction products from the salt decomposition step [Benjamin 1970].

Internal oxidation involves exposing metal powders or thin metal strip containing a dilute solid solution of a reactive element to an oxidizing environment at elevated temperatures. The reactive element is then converted into a dispersoid by diffusing oxygen [Chaston, 1945; Bonis and Grant, 1962; Spengler, 1964; Adachi and Grant, 1960]. It has been found experimentally that the particle size of the dispersoid increases with increasing depth of penetration of the internal oxidation front into the metal [Adachi and Grant, 1960]. Very fine, contamination-prone powders or expensive ultra-thin strips are required to obtain sufficiently fine dispersoid particle sizes. When the alloy also contains γ' forming elements, the oxygen potential has to be controlled to only oxidize the desired species.

In the selective reduction process an intimate mixture of metal oxides is produced and the oxide of the matrix alloy is selectively reduced leaving the dispersoid unaffected [Alexander *et al.*, 1961]. If Al and Ti are to be present in the matrix alloy, the reduction step is not possible with gases because of the stability of Al_2O_3 and TiO_2. These oxides can be reduced by the use of molten alkali and alkaline earth metals. However, this causes excessive growth of the dispersoid particles, and it is necessary to remove the reaction product oxides and carrier agent, usually a salt [Benjamin, 1970].

Mechanically alloyed ODS alloys are produced by deformation, a method which produces metal powder with controlled, extremely fine microstructures. The technique circumvents the shortcomings described earlier and permits the effective combination of oxide dispersion strengthening and γ' precipitation hardening in nickel-base superalloys. From the initial laboratory success in 1968 [Benjamin, 1970], the process has been developed into a well-controlled production operation. A range of nickel,

iron, aluminium and other alloys have been designed specifically for the process and techniques have been developed to form and fabricate the alloys into useful components [Benjamin and Volin, 1974; Weber,1980; Curwick, 1981; Gilman and Benjamin, 1983; Hack, 1984; McColvin and Smith, 1985; Arzt, 1988; Benjamin, 1988; Benn and Mirchandani, 1988; Whittenberger, 1989; Fischer and Weber 1990; Rühle and Korb 1991; Schaffer and McCormick, 1992].

2.2 Commercial MA–ODS Superalloys

There are two major commercial variants of MA superalloys (Table 1.1) the nickel-base alloys, intended for aerospace applications [Fleetwood, 1986; Sundaresan and Froes, 1987] and the more successful iron-base alloys for lower temperature applications. The density of the ferritic alloys is about 10 % lower than that of the nickel-base alloys, providing a significant strength/weight advantage, together with a lower thermal expansion coefficient which is beneficial when thermal fatigue is an important design criterion [Fischer *et al.*, 1977].

2.2.1 Iron–Base MA–ODS Alloys

There is growing technological interest in ferritic ODS alloys for possible use as heat exchanger process tubing, furnace and structural components. The alloys developed so far (Table 1.1) are designed to be oxidation and corrosion resistant, but with a greater creep strength when compared with equivalent cast alloys, due to the dispersion of fine yttria particles. MA956 has the greater oxidation resistance due to the high chromium concentration and its large aluminium content. Normal ferritic steels tend to undergo a marked loss in creep strength at temperatures in excess of 600 °C; the ODS alloys discussed here can in principle be used at much higher temperatures.

The excellent high temperature corrosion resistance of MA956 results principally from the formation of a stable, tightly adherent α–Al_2O_3 oxide coating. This oxide forms during the final heat treatment of mill products [Benn, 1983]. The high stability of dispersoids within the alloy matrix allows the

retention of usable strength at temperatures up to about $0.9T_m$ [McColvin, 1985].

Because of its formability, MA956 has been produced in the widest range of product forms of any mechanically alloyed ODS alloy. The alloy was originally developed for use in sheet form gas-turbine combustors, but with its combination of high strength up to 1300 °C, corrosion resistance and formability, the alloy has found a number of other applications. The gas-turbine applications under development include fabricated nozzles, compressor nozzle parts of vehicle turbines, rings for aero-engine combustors, and combustor baffle for industrial turbines. Use in power stations include oil and coal burners and swirlers, and fabricated tube assemblies for fluidized bed combustion. Burner flame stabilisers made from MA956 sheet and rivets are used in severely corrosive environments in which metal temperatures up to 1230 °C are experienced [Macdonald, 1981]. MA956 used in fliudized bed combustion has been evaluated successfully for local gasification in which its resistance to sulphidation and carburization is outstanding [Lloyd and Cooke, 1981]. The oxidation resistance of alumina forming MA956 is generally regarded as superior to that of materials which develop chromia scales [McColvin and Smith, 1987].

The ferritic iron alloys have been considered for fast-breader nuclear reactor structural materials because they do not embrittle at high temperatures and have lower swelling rate during neutron bombardment [Huet and Leroy, 1974]. Conventional ferritic steels are unsuitable because the operating temperatures of these reactors are around 650 °C. Carbide strengthening is not acceptable because carbon can be leached out or picked-up in a sodium environment. MA957 and a similar steel DT2203Y05 are therefore designed for nuclear reactor applications, for use in a liquid sodium environment at temperatures of the order of 700 °C. Both have a high void swelling resistances and a low carbon concentration in order to avoid the formation of titanium carbides [Asano *et al.*, 1988, Little *et al.*, 1991]. The titanium is meant to combine with chromium, molybdenum and iron to form a stable body centred cubic FeCrTiMo intermetallic χ–phase during ageing at around 800 °C, which can further boost the creep strength [Okafor and Carlson, 1978; Snykers and Huck, 1974].

The 'ODM' alloys are ferritic oxide dispersion microforged materials produced using the mechanical alloying technique. The compositions of ODM751 and ODM331 are very similar to MA956 alloy except that they contain 1.5 wt.% Mo with less chromium and more titanium. The rupture strength of ODM751 is larger than that of MA956 [Kazimierzak *et al.*, 1990]. The additional 1.5 wt.% Mo, either via the χ–phase or through solid solution strengthening, presumably adds to the creep strength of ODM751. However, the results are confusing because PM2000, which does not contain molybdenum, virtually matches the rupture strength of ODM751 [Bhadeshia, 1997]. The ODM alloys can be used for a wide range of high temperature applications including heat exchangers for advanced energy conversion systems, as well for chemical processes, gas turbines combustion chambers, diesel engine components, thermocouple shielding, resistors and other miscellaneous chemical applications.

PM2000 and PM2010 are ferritic MA–ODS superalloys. The former is claimed to show reduced pore formation during service and improved mechanical properties and weldability [Ruhl and Korb, 1991]. It shows a lower weight gain than MA956 during isothermal and cycling oxidation [Daeubler and Frischammer, 1990; Ruhle and Korb, 1991]. Results from tensile and stress-rupture tests as well as from oxidation and corrosion investigations are superior to those of other commercial ODS alloys [Daeubler and Froschammer, 1990]. PM 2000 can be used in gas-turbines (aircraft, marine, automotive etc.) combustion chambers, flame tubes, exhaust units, furnace construction, chemical processing equipments, glass and ceramic industries.

2.2.2 Nickel–Base MA–ODS Alloys

Incoloy MA754 and MA758 are nickel–base mechanical alloys without γ' strengthening. MA754 was the first mechanically alloyed ODS superalloy to be produced on a large scale. The material is basically a Ni–20 wt.% Cr alloy strengthened by about 1 vol. % Y_2O_3 (Table 1.1). It is comparable to TD–NiCr (an earlier ODS material strengthened with thoria, ThO_2) but has a non–radioactive dispersoid. The yttria dispersoid imparts exceptional high-temperature strength and creep resistance to the alloy. MA754 is used currently in military aircraft engines and offers an effective alternative to single crystal

castings and directionally solidified components [Fleetwood, 1986]. MA758 is a higher chromium version of MA754 (Table 2.1), developed for oxidation resistance. Its mechanical properties are similar to those of MA754 when identical product forms and grain structures are compared. MA758 has found applications in the metal processing industry and in the glass–processing industry.

The nickel–base alloys MA6000 and MA760 are both γ' strengthened. The dispersion strengthening with yttria allows the strength to be maintained to much higher temperatures. For example, at 1093 °C, the 1000 hour rupture strength of MA6000 is twice that of conventional nickel–base superalloys [Fleetwood, 1986]. For reasons which are not clear, the (low and high cycle) fatigue resistance of MA6000 is much better than that of conventional alloys, as is its thermal fatigue resistance [Gessinger, 1984].

A lot of the oxidation resistance of MA6000 relies on the formation of chromia at the surface. However, chromia is not very resistant to sulphidation. Resistance to sulphide attack is important in industrial gas turbine manufacture, where the ODS alloys have applications as vanes. MA760 has a higher sulphidation and oxidation resistance, due to its higher chromium and aluminium concentrations, the latter inducing the formation of surface alumina [Bhadeshia, 1997].

2.3 The Mechanical Alloying Process

The starting powders for mechanical alloying contain at least one ductile metal to act as a host or binder to hold the other ingredients together. They consist typically of a mixture of commercially available metal powders (or master alloy powders), fine refractory oxides and reactive elements. Since the use of elemental mixes in the starting powder often leads to the formation of inclusions of incompletely processed raw materials, pre-alloyed master alloy powders are preferred [Elliott *et al.*, 1991]. The pre-alloyed master alloy also reduces oxidation of reactive additives and the newly alloyed powder. Fine refractory oxides such as yttria are sometimes added to provide dispersion strengthening to $0.9T_m$ [Arzt, 1988]. Reactive elements (Ti, Al) provide oxidation resistance in the final product. In nickel-base

alloys, Ti and Al also provide intermediate temperature strength by precipitation of the γ', $Ni_3(Al, Ti)$ [Gilman and Benjamin, 1983]. The powders are produced in high-energy attrition mills or special large-ball mills, consolidated by various combinations of hot–isostatic pressing and extrusion and finally heat–treated, either isothermally or in a temperature gradient to induce recrystallisation (Figure 1.1).

2.3.1 High-Energy Milling

Mechanical alloying makes possible the combination of dispersion, solid-solution and precipitation strengthening by mixing all the constituents in powder form ever more intimately until the formation of a true alloy powder leaving only the oxides dispersed in the solid solution [Gilman and Benjamin, 1983]. Mixing is achieved by dry high-energy ball milling, under conditions which cause fragmentation and welding together, a process prevented in conventional ball milling by the use of liquids and surfactants.

During mechanical alloying, the particles become trapped between the colliding balls producing intense plastic deformation and fracture. The ductile metal powders are flattened and where they overlap, the atomically clean surfaces just created weld together, building up layers of composite powders and the dispersoid. At the same time work hardened elemental or composite powders fracture. A qualitative description of these repeated fragmentation and coalescence processes by Gilman and Benjamin (1983) is shown in Figure 2.1. The legends in Fig. 2.1 indicate the events that might occur depending on the impact angle. High strain–rate fracture is favoured for normal impact. Other modes such as forging fracture and shear fracture occur at glancing angles. Direct seizure is a coalescence event favoured by normal impacts. At other impact angles, indirect seizure (i.e, seizure preceded by sliding deformation) would be a preferred coalescence mechanism.

These competing processes of cold welding and fracture occur repeatedly throughout the milling, gradually kneading the composites so that their structure is continually refined and homogenised. The processes from the initial stage to the completion are schematically illustrated in Figure 2.2. After the initial stage of milling the composite shows coarse layers of identifiable starting materials, with the

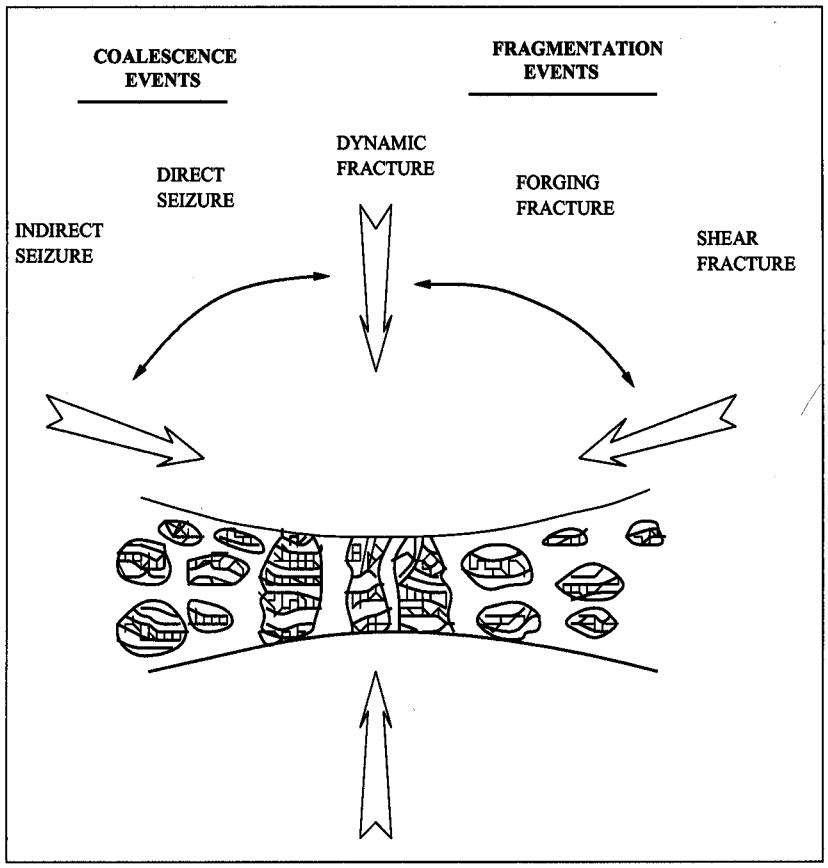

Figure 2.1 : Schematic illustration of the repeated fragmentation and coalescence processes in mechanical alloying [Gilman and Benjamin, 1983].

dispersoid closely spaced along the welds (Fig. 2.2a). After more refinement through fracture and welding, the composite develops a structure of convoluted lamellae of decreasing thickness between welded surfaces along which dispersoids are closely spaced (Fig. 2.2b). At this stage the average spacing of yttria dispersoids at the layer interfaces is similar to the average layer thickness resulting in an ideal random distribution of the oxide with an interparticle spacing of less than 0.5 μm [Hack, 1984]. The combination of severe cold-work and possible heating from the kinetic energy of balls aids diffusion and as diffusion distances decrease continually by the finer mixing of constituents, solute elements dissolve, areas of solid solution grow in composite powders and metastable phases may precipitate.

In the final stage of milling the lamellae become more convoluted and thin (Fig. 2.2c). The compositions of individual particles converge to the overall composition of the starting powder blend. Precipitation of

equilibrium phases may occur, work hardening and softening reaches a balance and the microhardness of the individual powder particles attains a saturation value of around 650 kg mm^{-2} for Fe–Cr alloys [Gilman and Benjamin, 1983]. Finally the lamellae are no longer resolvable optically and the distance between dispersoid particles along the weld interfaces, approximately equal to the spacing between the welds, (Fig. 2.2d). The composition of individual powder particles is then equivalent to that of the starting blend and mechanical alloying is said to be complete [Fleetwood, 1986].

The structures that develop during high energy ball milling of powders are dependent on the process variables and the nature of the powder components. These include the type and energy of the mill, the milling media, the milling temperature and atmosphere, the weight ratio of the powder to steel balls, the mechanical behaviour of the component powder mixtures and the chemistry and phase equilibra of the components [Koch, 1989].

The processing time for mechanical alloying depends upon the size and type of the mill used, the powder volume and the elastic constants of the powder [Courtney and Maurice, 1989]. It is not the number of ball/powder collisions but the energy absorbed per particle during a collision which controls the milling time [Aiken *et al.*, 1991]. Mechanical alloying processing times of 40 h or less are usually adequate for obtaining powder homogeneity [Benjamin, 1970].

To prevent uncontrolled oxidation of the metal powders, mechanical alloying is performed using inert process gas. Argon is the most popular gas [Kramer 1977] but some argon may become trapped during processing to precipitate later as very fine bubbles near the fine dispersoids [Jaeger and Jones, 1991, 1992b].

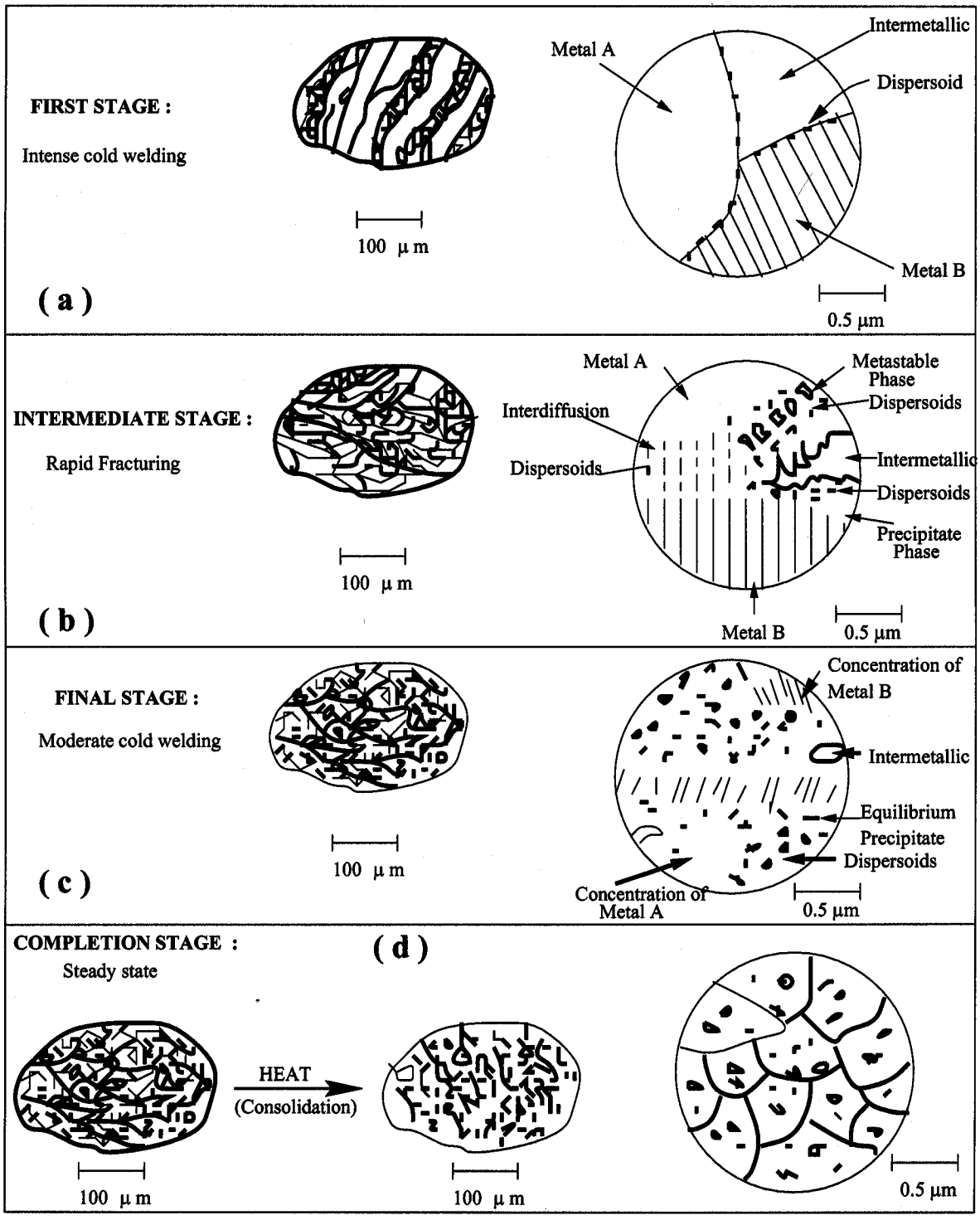

Figure 2.2 : Schematic illustration of the processes at different stages of mechanical alloying [Sundaresan and Froes, 1987].

2.3.2 Thermomechanical Processing

The presence of an oxide coating can inhibit metal powder from densifying on simple sintering [Gilman and Benjamin 1983] and the high hardness of mechanically alloyed powder prevents cold pressing. Therefore, the powder discharged from the mill has to be consolidated using high temperature and high pressure processes such as hot isostatic pressing (HIP), or heating in mild steel sealed cans followed by hot extrusion. The latter method is generally preferred as it is cheaper and able to produce anisotropic structures with good creep properties [Fleetwood, 1986].

The mild steel extrusion cans are filled from the 'alloy blend'. Cans of up to 280 mm diameter and 660 mm length are used, containing up to 170 kg of powder. Several hours of soaking in a furnace at the extrusion temperature is required to ensure that the centre of the powder mass is heated thoroughly. During this time inter–diffusion occurs which causes the highly strained composite powder particles to become chemically homogeneous with all the physical properties of a truly alloyed powder [Nutting *et al.*, 1981]. Extrusion is carried out in commercial 5000–6000 tonne presses at temperatures, reduction ratios and, speeds which are interdependent and which must be determined in conjunction with the subsequent hot-working parameters [Hack 1984]. After extrusion, the cans used for the consolidation are removed either by machining or by pickling, depending on the alloy and the product form.

The MA-ODS alloys in the as-extruded condition are usually too hard to use. They are therefore heat–treated, either isothermally or in a temperature gradient to induce recrystallisation. Recrystallization in MA–ODS alloys usually does not occur until temperatures close to melting are reached [Benjamin and Gilman, 1983; Gessinger, 1984; Hack, 1984]

2.4 Grain Morphology in MA–ODS Alloys

The major peculiar feature of the ODS mechanical alloys is that they tend to recrystallise into a highly anisotropic columnar grain structure. There are two reasons why such grain structures should

arise. Zone annealing, like directional solidification can encourage growth along the associated moving temperature gradient. Secondly, any dispersoids may tend to align along the extrusion direction, so that the Zener pinning force is smallest for growth parallel to the working direction, for both MA957 and MA956 [Chou and Bhadeshia, 1993].

For reasons which have never been explained, nickel–base alloys do not have a pronounced nonuniform distribution of dispersoids [Baloch and Bhadeshia, 1991]. Thus, MA6000, when isothermally annealed, often recrystallises into an equiaxed grain structure (there are batch–to–batch variations). The same alloy will recrystallise directionally when zone annealed. The sense of the columnar grains can be altered by changing the zone annealed direction; cross annealing (*i.e.* zone annealing in a direction normal to the extrusion direction) causes the growth of stubby columnar grains normal to the extrusion direction, confirming a more or less uniform dispersoid distribution. In addition, zone annealing at high speeds leads to a transition from a columnar to equiaxed recrystallised grains [Chou and Bhadeshia, 1993].

The nickel–base alloy MA760 has a response which is similar to that of MA6000, although the signs are that there is a stronger alignment of particles along the extrusion direction. Thus, isothermal annealing does not lead to equiaxed grains, but cross annealing can change the direction of the columnar recrystallised grains.

The mechanically alloyed steels contain a very pronounced alignment of particles along the extrusion direction [Baloch, 1989]. Isothermal heat–treatment of as–worked samples always leads to the development of coarse columnar grains. MA957, which has a rather low yttria content, has relatively stubby columnar grains following isothermal heat treatment. No amount of cross annealing or any other heat treatment has succeeded in causing a change in the direction of columnar grain growth, which is always parallel to the working direction. The importance of a nonuniform dispersion of particles in inducing the development of columnar grains has been emphasized in recent experiments where the introduction

of HfC or TiB_2 led to the formation of anisotropic grains during secondary recrystallisation of the NiAl intermetallic matrix [Jaeger and Jones, 1991].

The roughness of grain boundaries in recrystallised mechanically alloyed nickel–base superalloys and steels has been characterised in detail [Whittenberger, 1981; Jaeger and Jones, 1991; Murakami *et al.*, 1992]. The serrated boundaries arise because of transient pinning by dispersoids. Coarser and smoother boundaries occur when the stored energy is large, simply because it is then easier for the boundary to overcome the pinning force [Murakami *et al.*, 1992].

2.5 Preannealing Effects on the Recrystallization Behaviour of MA-ODS Alloys

Preannealing is a term used to describe a sample which has been heat treated at a temperature which is too low for recrystallisation, but high enough to induce significant changes in the stored energy, and in the subsequent microstructure following an elevated temperature recrystallisation heat treatment.

The effects of preannealing, at temperatures above that at which austenite can form, on MA957 can be summarised as follows [Chou and Bhadeshia, 1994]. A weak preannealing treatment (at about 1150 °C) has little or no effect on subsequent recrystallisation. As the preannealing time is increased, there is a transition from a coarse columnar grain structure to one which is equiaxed (20–40 μm) depending on the exact heat treatment). This is because the reduction in stored energy reduces grain boundary mobility, so that nucleation has an opportunity to develop in several regions of the sample, giving an equiaxed grain structure.

Continued preannealing causes the development of a bimodal equiaxed grain structure. This is because there is an inhomogeneous distribution of pinning particles in the alloy. The now substantial reduction in stored energy due to preannealing, retards recrystallisation more in some regions compared with others which are less strongly pinned. For MA957 the preannealing time at 1150 °C is in excess of 160 hours for this condition to be reached [Bhadeshia, 1997].

Further preannealing leads to such a large reduction in the stored energy that subsequent recrystallisation is suppressed.

It is much more difficult to control the grain structure of MA956 using preannealing heat treatments. Grain refinement certainly occurs, as in MA957, but the fine grains tend not to be equiaxed. This may be because MA956 contains a larger concentration of yttria. The anisotropic pinning due to the inhomogeneous distribution of the oxide particles is more difficult to overcome if the fraction of particles is large. It would be very interesting to test this with MA956 containing a smaller quantity of yttria dispersoids.

2.6 Initial Microstructures

Immediately after the mechanical alloying process, the powders are canned and extruded/hot–rolled to produce the appropriate bulk forms. During heating for either extrusion or rolling, the canned mechanically alloyed powders may recrystallise to a sub–micron grain size which is representative of the grain structure found immediately after consolidation. These incredibly fine grain sizes are a consequence of the strains imparted on the powders during the mechanical alloying process, true strains of the order of 9 (equivalent to stretching a unit length by a factor of 8000). The subsequent consolidation by comparison involves minor degrees of deformation, but much higher bulk temperatures (around 1000 °C). It is known that during the course of consolidation, the material may dynamically recrystallise several times. It should be emphsized that the sub–micron grains referred to above are true grains with large relative misorientations, not simply dislocation cell structures generated by deformation [Bhadeshia, 1997].

Nevertheless, the iron–base alloys immediately after consolidation have a cold–deformed microstructure in which the ultra–fine grains are elongated along the working direction and contain other classic features of cold work, *i.e.* the high dislocation density and a generally convoluted microstructure. The dislocation density has been measured for DT2203Y05 to be about 10^{15} m^{-2} [Little *et al.*, 1991]; although this is

large, it is not particularly high when compared with dislocation densities found in conventional steel martensitic microstructures . Subsequent heat–treatment leads to primary recrystallisation into a very coarse grained microstructure .

The nickel–base superalloys also have an ultra–fine grained microstructure, but one which is the product of primary recrystallisation . The sub–micrometer grains are therefore equiaxed, contain undistorted annealing twins and a clean microstructure. Subsequent heat treatment therefore leads to secondary recrystallisation driven by the grain boundary energy of the fine grained primary recrystallised state. It is not clear why the nickel base alloys are in a primary recrystallised state following extrusion/hot–rolling, whereas the iron–base alloys, which are fabricated under identical conditions, have a cold deformed microstructure.

Irrespective of whether the alloys have a primary or secondary recrystallised microstructure, the ultra–fine grains obtained after recrystallisation make the alloys very hard (Table 2.1) and for most applications unusable without heat treatment which leads to an enormous coarsening of the microstructure with a reduction in the amount of grain surface per unit volume by 2–3 orders of magnitude. The details of recrystallisation are discussed in the next section.

Table 2.1: Typical Vicker's Hardness data before and after recrystallisation into a coarse grained microstructure [Bhadeshia, 1997].

Alloy	HV, Before Recrystallisation	HV, After Recrystallisation
MA957	400–410	230–240
MA956	350–390	225–245
MA956 Sheet	410	250
MA6000	645	500–520
MA760	720–790	500–515
MA758	405	214

The excess energy stored in the mechanically alloyed and consolidated materials described in Table 2.1 is primarily in the form of grain surfaces and to a lesser extent due to dislocations and other high–entropy defects.

Extrusion/rolling leads to an alignment of dispersoid particles along the working direction, the degree of alignment being pronounced in the case of the iron–base alloys. This alignment reflects inhomogeneities in the fabrication process arising at the single particle level and below. Thus, the iron–base alloys almost always tend to recrystallise into a columnar grained microstructure, with the principal growth direction being parallel to the extrusion direction, irrespective of whether the sample is zone annealed, cross annealed or isothermally treated (cross annealing is zone annealing along a direction normal to the extrusion direction). For reasons which are not clear, the anisotropy in particle dispersion is much less for the nickel base superalloys, in which the direction of columnar grain growth can often be controlled by the sense of the temperature gradient during zone annealing. Indeed, equiaxed coarse grained secondary recrystallised microstructures can be readily generated either by isothermal annealing or by zone annealing at high speeds [Baloch and Bhadeshia, 1991].

2.7 The Dispersoids and Precipitates

Fine yttria particles ($\simeq$ 10 nm) are incorporated into the metallic matrix as a consequence of the ball milling operations. Most of these survive as yttrium oxide in spite of consolidation by extrusion and rolling at about 1050 °C. However, heat–treatment causes these particles to react with dissolved aluminium (or titanium) and oxygen to produce a variety of compounds [Krautwasser *et al.*, 1994; Murakami, 1993; Schaffer *et al.*, 1989; Cama and Hughes, 1993]. The possible combinations of yttria and alumina include those listed in Table 2.2.

The alumina particles tend to be some 500 nm in size, the titanium carbonitrides about 100–200 nm in size [Regle, 1994], and both have a much smaller number density than the original yttria particles. Hence, the reaction does not lead to a significant coarsening of the size distribution or inter–particle

Table 2.2: Yttrium–Aluminium–Oxygen compounds reported to occur in mechanically alloyed ODS iron and nickel base alloys.

$3Y_2O_3.5Al_2O_3$	YAG	yttrium aluminium garnet
$Y_2O_3.Al_2O_3$	YAH	yttrium aluminium hexagonal
$2Y_2O_3.Al_2O_3$	YAM	yttrium aluminium monoclinic
$Y_2O_3.Al_2O_3$	YAP	yttrium aluminium perovskite
$Y_2O_3.Al_2O_3$	YAP'	yttrium aluminium pseudo–perovskite
$3Y_2O_3.5Al_2O_3$	YAT	yttrium aluminite tetragonal

spacing. Even extremely severe heat–treatment (72 hours at 1400 °C) has little effect on the yttrium containing particles [Murakami, 1993]. Typical changes in the size of the finer particles are illustrated in Figure 2.3, which represents data for samples annealed for 110 h at the temperatures indicated, for samples of PM2010 [Krautwasser *et al.*, 1994]. Note that these data do not represent coarsening driven by interface energy minimisation, but complicated effects originating in the reactions between the yttria, aluminium and oxygen. Thus, the volume fraction is not constant during heat treatment. The volume fraction of the smaller reactive particles increases, whereas any large alumina particles tend to dissolve as the aluminium reacts with the yttria [Krautwasser *et al.*, 1994].

In the extruded condition, 80 % of the particles in both MA956 and MA957 are less than 15 nm in size, with those in MA956 being much smaller [Regle, 1994]. Nevertheless, the mean particle diameters are quite similar at 11.7 and 11.4 nm for MA957 and MA956 respectively [Regle, 1994], presumably because the fraction of particles is larger in the latter. Some typical particle sizes for the fine particles are presented in Table 2.3.

Table 2.3: Some particle characteristics, with the alloys in the unrecrsytallised "as–received" condition.

Alloy	Mean Particle Size / nm	Reference
MA957	12	Regle (1994)
MA956	12	Regle (1994)
PM2010	15	Krautwasser *et al.* (1994)

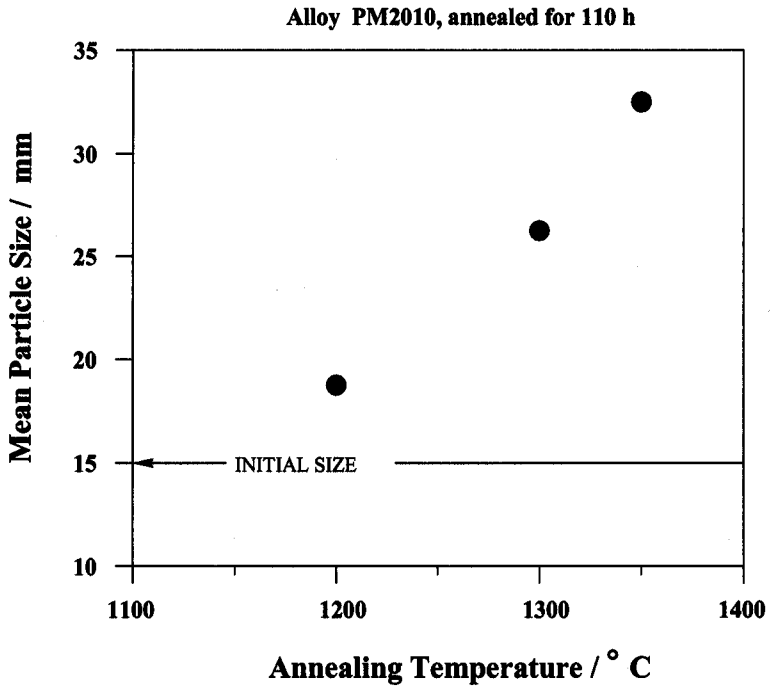

Figure 2.3 : Changes in particle size due to annealing, of alloy PM2010, for 110 h at each of the temperatures indicated. Data from Krautwasser *et al.*, (1994)

Almost all the mechanical alloys contain alumina particles introduced accidentally or as a consequence of internal oxidation during mechanical alloying (alumina is deliberately added to ODM751 at the mechanical alloying stage). These particles are also stable, but are too coarse and few to cause significant Zener pinning. Titanium containing mechanical alloys such as MA957 and MA6000 also contain titanium–rich particles whose exact character is not known; they may be oxides or carbo–nitrides.

The coarsest precipitates, which are not very stable, are the $M_{23}C_6$ particles which are visible optically, and dissolve (at around 1000 °C) during heating to the recrystallisation temperature only to reprecipitate during slow cooling to ambient temperature. These carbides are found in the nickel–base superalloys and not in the iron–base alloys which contain very low carbon concentrations.

To summarise, the yttrium based dispersoids are extremely stable in spite of some reaction with aluminium and oxygen to form garnets. The other particles are likely to be of little consequence to both

the recrystallisation process and the creep resistance of the alloys.

The mechanism by which the fine yttrium containing particles enhance the creep resistance has been studied both for the mechanically alloyed nickel–base superalloys and the steels [Nardone and Tien, 1983; Herrick *et al.*, 1988; Schroder and Arzt, 1985; Preston *et al.*, 1991]. The creep resistance arises from the fact that dislocations have to climb over the hard obstacles. For steels, the consequent improvement in creep resistance allows alloys such as DT2203Y05 to be used at a service temperature of 975 K compared with that for conventional ferritic stainless steels whose maximum service temperature is about 925 K.

For the steels, there is some evidence that the oxide particles and the intermetallic compounds which precipitate in some alloys, inhibit the migration of boundaries [Evans *et al.*, 1992].

2.8 Defects in Mechanically Alloyed Superalloys

Alloys produced by mechanical alloying always exhibit processing defects which include macro- and micro-porosity and inclusion particles. In addition, a peculiar defect called 'intrusion' has also been observed in MA alloys. Fine grains which result from incomplete recrystallization and particle denuded bands due to inadequate milling are also reported in MA ferritic ODS alloys. These defects are discussed below.

2.8.1 Macroporosity

All materials made by conventional powder metallurgy (PM) routes can contain coarse residual porosity usually situated at grain boundaries. Such pores are large and easily seen. Since MA products are subjected to a high level of mechanical working such macropores are unlikely to be retained but form subsequently due to the precipitation of dissolved gases.

2.8.2 Microporosity

During mechanical alloying, the fracture process exposes clean, fresh and rough surfaces which can adsorb gases. These gases, can become trapped between powder particles during welding and then be retained in solid solution. Jaeger and Jones (1991, 1992b) have reported micropores (between 0.1–0.2 mm) containing argon gas around second phase particles in ODM331 bar and tubes. According to Jaeger and Jones (1992b), the association of argon with particles can be due to the release of argon from high-angle grain boundaries that become pinned at particles while migrating during secondary recrystallization.

2.8.3 Intrusion Defects

These are defects observed only in MA-ODS alloys [Cama, 1994]. They are equiaxed and filled with material of matrix composition similar to that in the micro-wrought pre-consolidated powders [Zeizinger and Arzt, 1988; Weisbrodt *et al.*, 1990; Jaeger and Jones, 1991]. The defects are surrounded by discontinuous layers of "debris" in the form of Al-, Y- and Ti-rich particles and their bonding with the surrounding matrix is weak [Korb, 1988]. Intrusion defects pin grain boundaries and hence hinder recrystallization [Jaeger and Jones, 1992b]. They also hamper transverse grain growth [Cairns *et al.*, 1975, Jongenburger and Singer, 1988]. Intrusion defects can be minimized by using clean raw materials and master alloys, avoiding contamination during powder handling, controlling milling parameters and by monitoring the mechanical alloying process very carefully to eliminate any under processed particles [Schneider and Dannhauser, 1991].

2.8.4 Bands of Fine Grains

In many MA superalloys, recrystallization may not reach completion, leaving elongated regions of fine-grained materials [Cairns *et al.*, 1975]. These regions can reduce creep performance [Zeizinger and Arzt, 1988; Jaeger and Jones, 1992b]. The defects have been observed in MA ferritic alloys and ODM751 [Jaeger and Jones, 1992b] and in nickel-base MA6000 [Arzt, 1988; Weisbrodt *et al.*,

1990]. Randomly distributed fine grains (length about 1 mm), depleted of dispersoids have also been recently reported in an experimental iron-base ODS alloy DYAL (with nominal composition : 13Cr–3Al–1.5Mo–0.6Ti–0.5Y_2O_3) similar to ODM751 [Kehagias *et al.*, 1993].

2.8.5 Particle Denuded Bands

Particle-denuded bands are a consequence of inadequate milling due to "dead zones" in the mills used for mechanical alloying. Jaeger and Jones (1992b) have reported dispersoid-free zones in ferritic MA–ODS alloys, ODM331 and ODS751. Kehagias *et al.*, (1993) also reported similar particle denuded bands (of width approx. 2 mm) in an experimental ferritic ODS alloy DYAL. These regions are weak and can act as centres for strain localisation during deformation [Jaeger and Jones, 1992b].

2.9 Strengthening in ODS Alloys

Strengthening in ODS alloys is achieved by dispersoid particles acting as barriers to dislocation motion during deformation and as a result increasing the load required to tear away a dislocation or bulge it through an array of particles. Here the strengthening can be described by the various mechanisms by which dislocations interact with or by-pass the obstacles. For optimum dispersion strengthening, distributing a given volume fraction of dispersoids more finely is more effective than increasing the volume fraction [Benn and Mirchandani, 1988; Rosler and Arzt,1990]. The ability of dispersoid phases to impede dislocation motion at elevated temperatures has also been related empirically to their free energies of formation, $-\Delta G_f$ [Benn and Mirchandani, 1988]. Refractory oxides such as zirconia, alumina and yttria (stability in increasing that order) have $-\Delta G_f$ values several fold higher than γ' or metal carbides and thus offer more stable configurations [Lawn *et al.*, 1976; Lupis, 1983; and Elliott, 1991].

In addition to acting as barriers to dislocation motions, particles also exert a retarding force on migrating grain boundaries. The retarding force per unit area, F_r, is according to Zener, (1948), given by:

$$F_r \simeq \frac{3f\gamma_{gb}}{2r} \tag{2.1}$$

where f is the volume fraction of particles of uniform radius r and γ_{gb} is the grain boundary energy per unit area [Martin and Doherty, 1980]. Hence, for a given volume fraction of particles, the smaller particles offer a greater hindrance to the migrating grain boundary compared to that offered by the larger particles.

2.9.1 Dislocation–Particle Interactions

There are several ways in which fine particles can act as barriers to dislocations. They can act as strong impenetrable particles through which the dislocations can move only by sharp changes in curvature of the dislocation line. On the other hand, they can act as coherent particles through which dislocations can pass, but only at stress levels much above those required to move dislocations through the matrix phase. There are four essential ways by which dislocations overcome particles that are present on their slip planes:

(i) Orowan bowing;

(ii) cross-slip;

(iii) climb over particles;

(iv) particle shearing.

Dislocation bowing and cross–slip occur for $T < 0.5T_m$, where T is the absolute temperature of deformation and T_m is the melting point. According to Orowan (1946), when a dislocation encounters two particles on its glide plane, it expands in the region between them until the segments on either side of the particle meet and form a dislocation loop around the particle. Dislocations may not always be confined to their slip planes during the bowing out process since cross-slip can occur. When by-pass is complete, residual loops remain associated with the particle [Wilcox and Clauer, 1972a]. According

to Ashby (1969), the initial flow stress of dispersion strengthened crystals is most probably controlled by Orowan by-passing rather than cross slip. The situation may be more favourable for cross slip to occur if Orowan loops are left first or if misfits strains around the particles exist which might be developed during cooling from high temperature owing to differences in thermal contraction [Singer and Gessinger, 1984]. Cross slip becomes more difficult as the stacking-fault energy is decreased. This is because of the additional force which is required to constrict a more widely split dislocation before cross slip can occur [Singer and Gessinger, 1984]. Chrumium additions decrease the stacking-fault energy in Ni-Cr alloys [Beeston and France, 1968]. Thus cross slip is expected to be unlikely in alloys with high chromium concentrations.

High temperatures enable dislocations to overcome the oxide particles by thermally activated climb, while at low temperatures where diffusion is slow, dislocation by-pass is assumed to occur by Orowan looping. If the spacing of the particles is small, then the applied stresses cannot bend the dislocation to a radius comparable to the particle spacing and the dislocations shear the particle. Also if a dislocation bows around a particle, especially a soft one, it is possible that the particle will be sheared as an alternative [Wilcox and Clauer, 1972b].

In dispersion strengthened alloys the overall material strength has contributions from both the matrix grain structure and the second phase dispersion.

2.9.2 Matrix Strengthening

In polycrystalline materials grain refinement represents a very useful and economical method of improving both the strength and fracture resistance. At low temperatures, the yield strength, σ_y, of a material is related to its grain size, d, by an empirical expression originally proposed by Hall (1951) and greatly extended by Petch (1953). The expression, which is known as Hall-Petch equation, has the form given as :

$$\sigma_y = \sigma_i + k_o d^{1/2} \tag{2.2}$$

where σ_i is the "lattice friction stress" which is temperature dependent and represents the overall resistance of the crystal lattice to dislocation movement, and k_o is the "locking parameter", a constant which is independent of temperature, composition and strain rate and reflects the difficulty in spreading slip across the grain boundaries. k_o measures the relative hardening contribution of the grain boundaries.

2.9.3 Dispersoid Strengthening

The strengthening from dispersoids comes from the need to move the dislocations past the particles. The resolved shear stress (τ_p) required for dislocation by-pass according to the Orowan (1946) model is

$$\tau_p = \frac{K'Gb}{\Lambda} \tag{2.3}$$

where G is the shear modulus of the matrix, b is the magnitude Burgers vector of the dislocation, Λ is the interparticle spacing and K' is a numerical constant. Ashby (1966) modified the Orowan model to take account of the interaction between neighbouring dislocations which had bowed, the line energy of the dislocations and the interparticle spacing. His model resulted in a reduction of the applied stress required for by-passing to occur.

$$\tau_p = \frac{K''Gb}{\Lambda} \ln\left(\frac{\bar{x}}{2b}\right) \simeq k'''\Delta\sigma_y \tag{2.4}$$

where $\bar{x}$ is the average diameter of the circle of intersection between the particle and the slip plane, $\Delta\sigma_y$ is the increase in the tensile stress for dispersion–strengthened alloys with uniform spherical particles and K''' is a constant.

Assuming that hardness H is proportional to the yield strength, it follows that

$$H = H_m + k_p d^{-1/2} \tag{2.5}$$

where H_m is the hardness of the matrix and k_p is another constant [Ashby and Jones, 1980]. For a fixed volume fraction of dispersed particles, the hardness should increase with decreasing particle diameter and for a fixed particle size, the hardness should increase with increasing volume fraction

of dispersoids. Therefore strengthening is increased if the volume fraction of dispersoids is high, the particles are fine, the particle distribution uniform and for high temperature applications, the particles inert [Tien and Purushothaman, 1976].

2.10 Effects of Grain Shape and Particle Distribution on the Creep Properties of MA–ODS Alloys

The grain structure developed in MA–ODS alloys depends strongly on the thermomechanical processing history. Either grain structures which have micron or submicron scale grain size, or very coarse secondary recrystallized grain structures with high GAR can be produced. A high aspect ratio grain structure can be produced over quite short distances in a sufficiently steep stationary temperature gradient. Alternatively, extremely high aspect ratio structures can be developed a length of 1 m or more by the application of a moving hot zone annealing technique [Cairns, *et al.*, 1975; Benn *et al.*, 1981].

The development of high GAR structure in ODS materials can also be influenced by the range of inert particles present in the alloy; these particles may be strengthening or non-strengthening depending on their size. Incorporation of a dispersion strengthening phase can improve the elevated temperature performance of alloys. However, the improvement in strength can depend strongly on the size, distribution and type of particle present.

2.10.1 Effect of Grain Aspect Ratio (GAR)

The good high-temperature properties of ODS superalloys correlate directly with their coarse elongated grain structures [Wilcox and Clauer, 1972; Benjamin and Bomford, 1974]. The grain aspect ratio (GAR) of a material is the average length to breadth ratio of the grains. Wilcox and Clauer (1972) found that the creep and yield strength at 1093 °C in nickel based thoria dispersion strengthened alloys increased linearly with increasing GAR. Similarly, as illustrated in Figure 2.4, Benjamin and Bomford, (1974) reported that elevated temperature mechanical properties of an experimental MA753 are proportional

to the grain aspect ratio up to about 6:1. In practice, a minimum grain aspect ratio of 8:1 is normally considered acceptable [Hack, 1984].

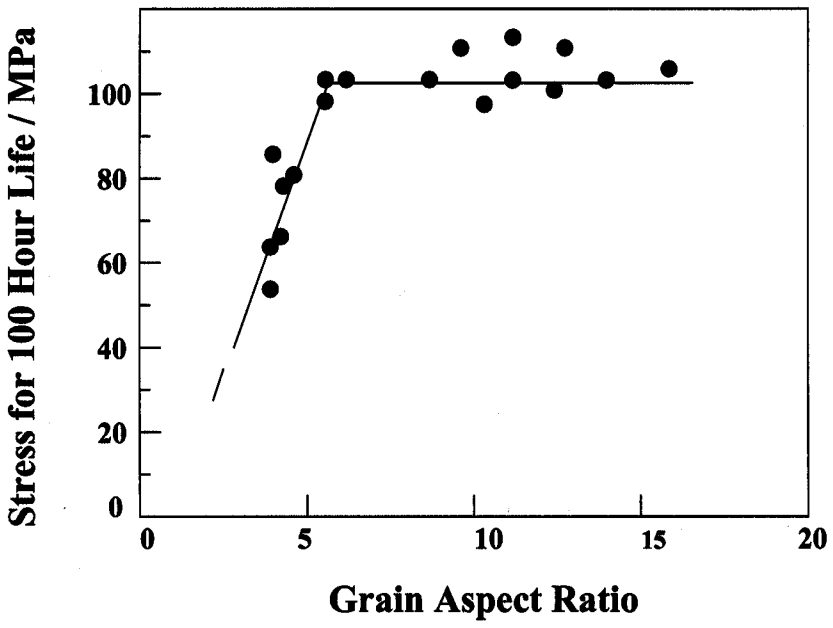

Figure 2.4 : Relationship between 100 hrs life at 1038 $^{\circ}C$ and grain-aspect ratio in experimental INCOLOY alloy MA753 [Benjamin and Bomford, 1974].

A high GAR can in principle improve the creep properties in the following ways:

(i) inhibition of creep damage accumulation;

(ii) retardation of diffusional creep;

(iii) retardation of grain boundary sliding.

Wilcox and Clauer (1972) suggested that the increased creep and yield strength with increasing GAR in thoria dispersion strengthened nickel based alloys was due to retardation of grain boundary sliding.

Reducing grain boundary sliding through the control of GAR has been postulated as the reason for the improved creep strength observed by Arzt (1984) in tests on MA 6000. Arzt tested materials with different GAR ranging from 4 to 60 at 950 °C and showed that the time to rupture showed a pronounced

dependence on the GAR. Below a value of 15, fracture was mainly intergranular, whereas at higher values of GAR rupture times became less sensitive to GAR, and failure was mainly transgranular. It was suggested that at values of low GAR grains readily slide past each other and intergranular fracture by cavity growth can occur unimpeded. As the GAR increases, sliding is impeded and cavity growth is retarded. Arzt (1984) suggested that a threshold stress exists below which sliding does not take place. A threshold stress of 6 MPa was given for the MA6000 tested.

Other work on MA6000 by Zeizinger and Arzt (1988) revealed that the transition between intergranular and transgranular failure was at a GAR of about 18, showing good agreement with that found by Arzt (1984). However, experiments to determine the cavity growth accommodation mechanism revealed that, contrary to the above, grain boundary sliding did not control creep damage accumulation. In fact, a mechanism based on dislocation creep was suggested to be rate-controlling. The authors proceeded to develop a model for time to fracture as a function of GAR in which the decisive parameter for creep accommodation necessary for cavity growth was the GAR. In the derivation of the model they assumed no grain boundary sliding, and that damage accumulation was by dislocation creep. From this it seems that the main parameter determining accommodation of damage should be one based upon inhibition of dislocation movement rather than one based on GAR. Nevertheless, the model agrees well with experimental observations by Zeizinger and Arzt (1988) and by Wilcox and Clauer (1972).

As the GAR of a material increases, the shear stresses on longitudinal grain boundaries are reduced and accommodation by grain boundary sliding becomes more difficult. However, high GAR is not the only factor to play a significant role in preventing sliding. Grain boundary particles can inhibit the movement of grain boundary dislocations and may be poor sources and sinks for vacancies. As grain boundary sliding takes place by movement of grain boundary dislocations then grain boundary particles will restrict dislocation movement and inhibit sliding.

The capacity of grain boundaries to slide may also be influenced by the level of texture developed

within the alloy. Sellars and Petkovic-Luton (1980), found that the degree of crystallographic texture increased with GAR. So these may not be independent parameters. Lund and Nix (1976) identified that an increased degree of texture leads to a prevalence of grain boundaries of low misorientation. These low misorientations or low angle boundaries could be less favourable sources and sinks for vacancies than more general high angle boundaries. Low angle boundaries are also less likely to undergo grain boundary sliding. Zeizinger and Arzt (1988) have further suggested that it is not the grain aspect ratio which determines the accommodation of damage but rather the interlocking between individual grains. This increases with the GAR. It is difficult however, to see how the serrated nature of the grain boundary is directly related to the GAR which is governed by a combination of the level of prior deformation, loading and the size and distribution of second phase particles. For example, work by Sellars and Petkovic-Luton (1980) showed that, with increasing GAR, the grain boundaries tend to lie preferentially along stringers of high oxide content. It is most likely that the particles will play the dominating role in determining the level of grain boundary serration and not the GAR.

2.10.2 Effect of Second Phase Particles

The presence of a uniform dispersion of fine inert particles provides an effective barrier to dislocation movement in ODS materials. Thorium oxide (ThO_2) was selected as the dispersoid phase for early alloys but yttria gives a better distribution during mechanical alloying and unlike thoria is not radioactive.

It might be assumed that an increase in the yttria content should lead to a corresponding increase in the creep resistance. This must be the case as the concentration is increased from zero, but recent work [Krautwasser *et al.*, 1994] indicates that there may be an optimum concentration of yttria. In a series of experiments carried out on alloys PM2000 and PM2010, which differ only in the yttria content (0.5, 1.0 wt.% respectively), it was found that the higher quantity in PM2010 does not lead to a significantly larger number density of fine dispersoids (< 100 nm). It was predicted therefore that PM2010 should not have a higher creep strength than PM2000 [Krautwasser *et al.*, 1994]. This result remains to be verified.

The volume fraction and size of particles chosen can vary from alloy to alloy and from one product to another. Typical concentrations (wt.%) and particle sizes of Y_2O_3 in a number of ODS alloys are given below in Table 2.4.

Table 2.4 : Size and wt.% of dispersoid in MA–ODS alloys.

Alloy	Product form	Y_2O_3 (wt.%)	Y_2O_3 (size, nm)	Reference
MA956	Sheet	1.2	250	Whittenberger (1978)
MA956	Bar	0.58	30	Haghi (1990)
MA754	Bar	1.3	5-100	Howson (1980)
MA6000	Bar	2.5	100	Zeizinger (1988)

In addition to the strengthening phase, MA–ODS alloys usually contain distributions of other, coarser dispersoids, which have either been carried through to the final product as part of the processing route or have been precipitated during processing. Examples of these coarser dispersoids are given below in Table 2.5. The size and volume fraction of fine dispersoid can affect the evolution of microstructure and the elevated temperature strength of ODS alloys. Benjamin and Bomford (1974) examined the effect of dispersoid volume fraction in a Y_2O_3 strengthened, nickel-base superalloy. The volume fraction of dispersoid added ranged from 0 to 0.045 while the size ranged from 15–58 nm. The combination of high volume fraction and small particle size produced an alloy with a low GAR and poor stress rupture properties at both 1038 °C and 760 °C. Apart from this, the stress rupture strengths at 760 °C were insensitive to variations in particle size and volume fraction. However, the dispersoid greatly affected the GAR [Benjamin and Bomford, 1974]. This in turn, influenced the rupture properties. For GAR less than 6 the 1038 °C ruptured strength was controlled by GAR while at higher GAR it was found to be controlled by a dispersoid parameter ratio f/f_a, where f is the volume fraction and f_a is the volume

Table 2.5 : Typical coarse oxides found in MA–ODS alloys.

Alloy	Product form	Dispersoid type	wt.%	Size (nm)	Reference
MA956	Sheet	$Spinel + Cr_2O_3$ $Cr_2O_3 + Y_2O_3$	2.0	450	Whittenberger *et al.*, (1978)
PM2000	Bar	Al_2O_3 $Al_2O_3 + Y_2O_3$	0.80	360	Jaeger (1994)
MA754	Bar	$Ti(CN)Al_2O_3$ $Y_2O_3Al_2O_3$	-	100-900	Howson *et al.*, (1980)
ODM751	Tube	$Ti(CN)Al_2O_3$ $Y_2O_3Al_2O_3$	0.6	300	Jaeger (1994)

average of the oxide particle size.

2.11 Threshold Creep Stress in MA–ODS Alloys

The elevated temperature deformation behaviour of ODS alloys is characterized by a threshold stress below which the creep rate is negligible. Whittenberger (1977) observed threshold stresses of around 53 MPa for thoria dispersion strengthened nickel and thoria dispersion strengthened NiCrAl tested at 1100 °C. He also observed that for MA754, the threshold stress was dependent on the GAR with the threshold value of 72 MPa for materials with a GAR of 3.5 tested parallel to the extrusion direction and 17 MPa when tested in the long transverse direction where the GAR was < 1. Petkovic-Luton *et al.* (1983) also found a threshold stress of around 70 MPa in single crystal MA956 tested between 1050 and 1150 °C while Haghi and Anand (1990), ascribed a threshold stress of 31 MPa to MA956 tested at 900 °C.

The existence of a threshold stress has been attributed to a number of mechanisms including :

(i) repulsive dislocation-particle interactions;

(ii) dislocation-particle interactions involving localized climb;

(iii) attractive dislocation-particle interactions.

The repulsive dislocation-particle interaction mechanism involves dislocations either looping the particles, as in the Orowan mechanism described previously, or by dislocation climb. In each case the threshold stress is the stress required for dislocation by-pass.

Evidence for Orowan dislocation interactions has been observed by Haghi and Anand (1990), who found dislocation loops around yttrium oxide dispersoids in MA956 tested at 1000 °C. However, they also found that the measured threshold stress was only about half the calculated Orowan stress. They concluded that the threshold stress is due to a combination of repulsive and attractive dislocation particle interactions. Further work by Petkovic-Luton *et al.* (1983) on the same material found no evidence of dislocation loops or debris expected from an Orowan mechanism.

It would appear, therefore, that the Orowan stress cannot be identified with the values of threshold stress found in ODS alloy system. This has led to the development of models based on processes by which dislocations can cirumvent particles, especially by climb. One such process proposed by Brown and Ham (1971) assumed that dislocation climb is local, *i.e.,* is confined to the portion of the dislocation close to the particle/matrix interface. This segment undergoes climb while the remaining dislocation line stays in the glide plane. Climb by-pass of dispersoid particles leads to an overall increase in dislocation line length. The increase in line length necessary to surmount the particle needs an increase in energy and this is provided by the applied stress. A threshold stress must be exceeded before the energy requirements are achieved and localized climb occurs. Arzt and Wilkinson (1986), however, suggested that the sharp dislocation curvature necessary for localized climb cannot be sustained at the point of dislocation–particle contact as it would rapidly relax by diffusion, leading to more general climb. A threshold stress would still exist from the general climb of dislocations but this has been estimated by Shewfelt and Brown (1977) and Arzt and Ashby (1982) as less than 10 % of the Orowan stress.

2.12 Elevated–Temperature Failure in ODS Alloys

The failure mode in ODS materials operating at elevated temperatures depends on a number of parameters such as the operating temperature, strain rate and microstructure. Whereas a fine grained ODS alloy may show superplasticity, the same alloy tested under identical conditions but in coarse grained secondary recrystallized condition is likely to fail by cavity formation. For example, Wiegert and Henricks (1980) tested secondary recrystallized MA 956 and a developmental iron-base alloy HDA8077, and found that a critical strain rate of 5×10^{-3} min^{-1} existed above which the materials had high ductility and failure was by microvoid coalescence. However, below the critical strain rate the material failed intergranularly, through cavity linkage, with low ductility.

There is a large body of evidence to indicate that under typical creep and stress rupture conditions, failure of ODS alloys, in the secondary recrystallized condition, is governed largely by the ease with which creep cavities nucleate, grow and eventually coalesce. For example, Howson *et al.* (1980) showed that MA754 failed by intergranular cavitation at grain boundaries transverse to the applied stress when creep tested in the temperature range 760–1093 °C. Zeizinger and Arzt, (1988) showed that when creep testing MA6000 at 850 and 950 °C the developing fracture modes changed from mainly transgranular to intergranular when the grain aspect ratio was greater than 18 with both failure mechanisms strongly influenced by cavity formation. Failure by cavity formation has also been observed in iron-base ODS materials by Wiegert and Henricks (1980) who tested MA956 bar at 1093 °C at a strain rate of between 10–9 and 10–5 min^{-1} and by Whittenberger (1978) and (1979) who creep tested MA956 sheet and bar at 1100 °C.

2.12.1 Creep Cavity Nucleation

Nucleation of a cavity always occurs where deformation is inhomogeneous [Goods and Brown, 1979]. In non-particle hardened systems this takes place at the grain boundary triple points, grain boundary irregularities or blocked slip bands. Homogeneous cavity nucleation by vacancy accumulation is

considered improbable at high temperatures as the vacancy supersaturation necessary to form the void would probably not be achieved during deformation [Balluffi and Seigle, 1955]. Nix (1982) has indicated that even if diffusion processes were not a factor in limiting supersaturation, normal stresses in excess of yield strength of YS/100 GPa, would be necessary to provide sufficient supersaturation to nucleate a void. These stresses can not be achieved by the applied stresses alone.

In ODS materials cavity nucleation is associated with dispersoids. Goods and Brown (1979) have suggested that nucleation can take by mechanical decohesion between the particles and the matrix. This mechanism is favoured by most researchers such as Harris, (1965), Rukwied (1973) and Fleck *et al.* (1975). It involves the particle behaving as a discontinuity in the boundary plane and acting as a stress concentrator in the event of grain boundary sliding. Cavitation results either from rupture of the particle or the particle/matrix interface.

Creep cavity nucleation may also occur through intense thermomechanical processing. For example, Pilling and Ridley (1988) suggested that the association of cavities with particles in the superplastic materials can be related to pre-existing defects such as regions of particle/interface decohesion. These are believed to have developed during the intense thermomechanical processing applied to a material in order to produce the fine grain sub–grain superplastic microstructure.

2.12.2 Cavity Growth

A cavity whether pre-existing or nucleated by vacancy condensation at a particle/matrix interface or by plastic flow of the matrix, can grow by a number of mechanisms. If grain boundary sliding is the mechanism for cavity nucleation, it seems reasonable that continued sliding should lead to continued cavity growth. The evidence, however, does not wholly support this, since cavities often appear to be reasonably uniform in size across a grain boundary facet whereas the sliding displacements are usually non-uniform [Evans and Wilshire, 1985].

Although it is unlikely that vacancy diffusion alone can nucleate cavities at high temperatures, diffusion

produces cavity growth. Figure 2.5 shows schematically the mechanisms which can cause cavity growth at high temperatures. These are: diffusion-controlled (a and b); and dislocation creep-controlled (c) [Arzt, 1984]. Growth by diffusion is stress directed with the tensile stress component governing the diffusion process. Where boundary diffusion alone controls growth (Fig. 2.6a) matter diffuses out of the growing void and deposits onto the grain boundary. The void is assumed to maintain its spherical shape during growth because surface diffusion is generally fast compared to grain boundary diffusion. This assumption may not be wholly justified under conditions where void growth is controlled by surface diffusion (Fig. 2.6b). When surface diffusion is slow, the void ceases to grow as a sphere. Matter from the cavity tip diffuses into the boundary at a rate which is faster than can be replaced by diffusion from other parts of the cavity surface. The void then becomes flatter and more crack-like.

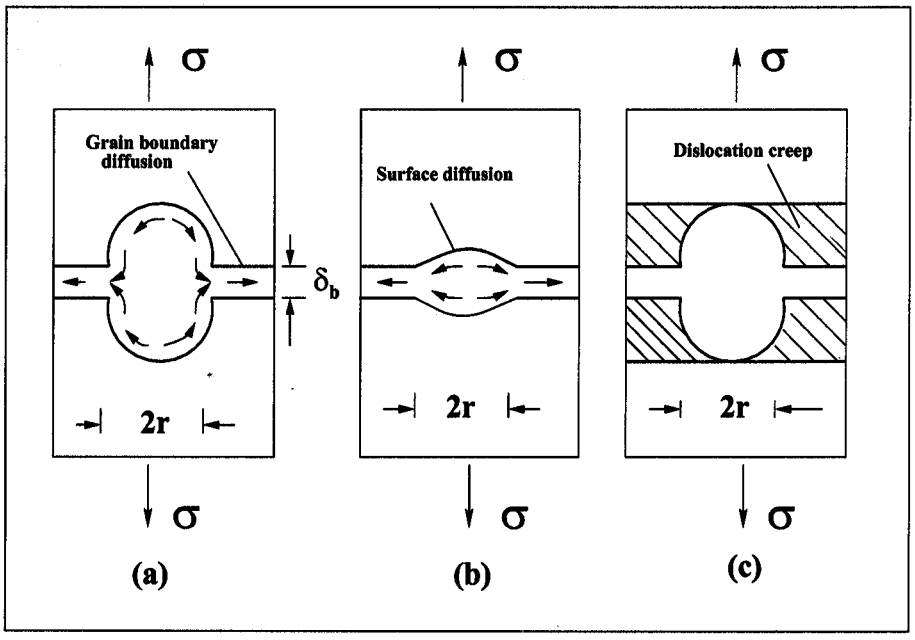

Figure 2.5 : Schematic of cavity growth mechanisms [Arzt, 1984]. (δ_b is the gap between boundaries, $2r$ is void size)

2.12.3 Constrained Cavity Growth

The cavity growth models described earlier generally assume that the total load on each grain boundary is constant, implying that each grain is free to slide and that no constraints exist. Dyson (1976), however, proposed that in a polycrystalline material cavity growth is constrained by the ability of neighbouring grains to accommodate shape changes and maintain contiguity by dislocation creep or grain boundary sliding. This mechanism of constrained cavity growth assumes that cavitation is a continuous process, with grain boundaries having different cavity nucleation rates. Hence a cavitated grain boundary can be surrounded by uncavitated grain boundaries. Such inhomogeneous distributions of grain boundary cavities have been observed by Tipler *et al.* (1970) from an examination of creep fracture surfaces. The mechanism of constrained cavity growth can be explained through Figure 2.6, where cavitation at the boundary between grains A and B has caused the grains to move apart. Cavity free grains C and D however do not move apart and a compressive stress can build up at EF.

This build up of compressive stress can be relieved by material diffusion or by plastic flow of the grain interiors. Then cavities will grow by a rate determined by the specific stress relaxation mechanism. At low stresses the relief mechanism is by diffusional creep while at higher stresses grain interior dislocation creep dominates. The relief of compressive stresses is easiest with dislocation creep and cavity growth is more rapid. However, if the grain interior is resistant to dislocation creep, as is the case for ODS materials, then diffusional relief mechanism will dominate. Similarly if the grain boundaries are not free to slide, as may be for MA–ODS materials with highly serrated grain boundary topography, then cavity growth will be limited.

2.12.4 Accommodation of Creep Damage

A grain boundary cavity grows by the displacement to material within the microstructure. This displacement of material needs to be accommodated to maintain compatibility and can be achieved by the mechanisms described in the previous section, namely; grain boundary sliding; stress directed diffusion;

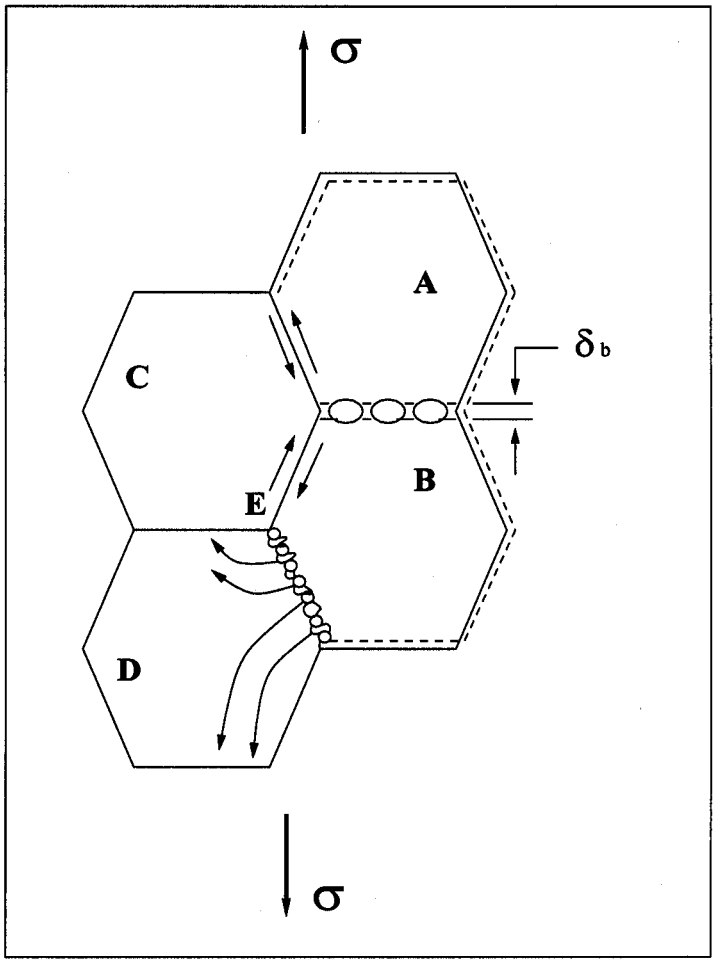

Figure 2.6 : Schematic diagram of constrained cavity growth mechanism (Dyson, 1976).

or dislocation creep of the surrounding matrix. More reasonably, the accommodation mechanisms are likely to be a combination of the above, as indicated by Raj and Ghosh, (1981) and Timmins and Arzt (1988). These accommodation mechanisms may also control the rate of cavity growth so, by limiting one or more of these mechanisms cavity growth will be limited and the creep strength will be increased.

In ODS materials dislocation creep is strongly suppressed by the effectiveness of the dispersoid in resisting dislocation motion. This will therefore limit the growth of cavities in a situation where the dislocation creep of the material surrounding the cavity is rate controlling. In addition, for some MA–ODS alloys, for example, MA6000, examined by Arzt (1988), where thermomechanical processes have produced a highly elongated grain structure containing serrated grain boundaries, grain boundary

sliding is limited by the keying in of the serrations and, therefore, cavity growth controlled by sliding is also limited. Grain boundary sliding is further inhibited as the resolved shear stresses necessary for sliding will be greatly reduced when the grain boundary is aligned parallel to the stress direction, as is the case for alloys with high GAR. Cavity growth by stress directed diffusion of vacancies may also be inhibited when the grain size is large because the diffusion distances between vacancy sinks and sources are large. This reduction in diffusional creep can become even more evident when the coupled with the inability of grain boundaries to slide [Nix, 1981]. Inhibition of growth of cavities by serrated grain boundaries is only applicable where the applied stress and other factors favour sliding. For alloys where the long axis of the developed high GAR grain structure is aligned parallel to the applied stress, where the resolved shear stresses are low this is not a problem. However, some engineering applications require loading where the short axis of the elongated grain structure is aligned with the stress axis, for example, internally pressurised tube. Here cavities will form on longitudinal grain boundaries and the transverse boundaries will need to be serrated in order to resist sliding and limit cavity growth. In this case the problem may be exacerbated as the transverse boundaries are often observed to be nearly aligned to the maximum principal shear stress.

2.13 Anisotropic Mechanical Behaviour in MA–ODS Alloys

Oxide dispersion strengthened alloys produced by mechanical alloying have been found to show anisotropic mechanical behaviour with the strength along the transverse direction lower than that along the extrusion or rolling direction.

Whittenberger, (1981) investigated the elevated temperature tensile properties of MA956 bars and their results are as shown in Figure 2.7. The longitudinal direction was shown to be stronger with greater ductility than the transverse direction.

Alamo *et al.* (1992) evaluated the tensile strength of 25 % cold-worked bars of MA957 and a summary of their data on the proof stress (PS) and ultimate tensile strength (UTS) measured in the longitudinal

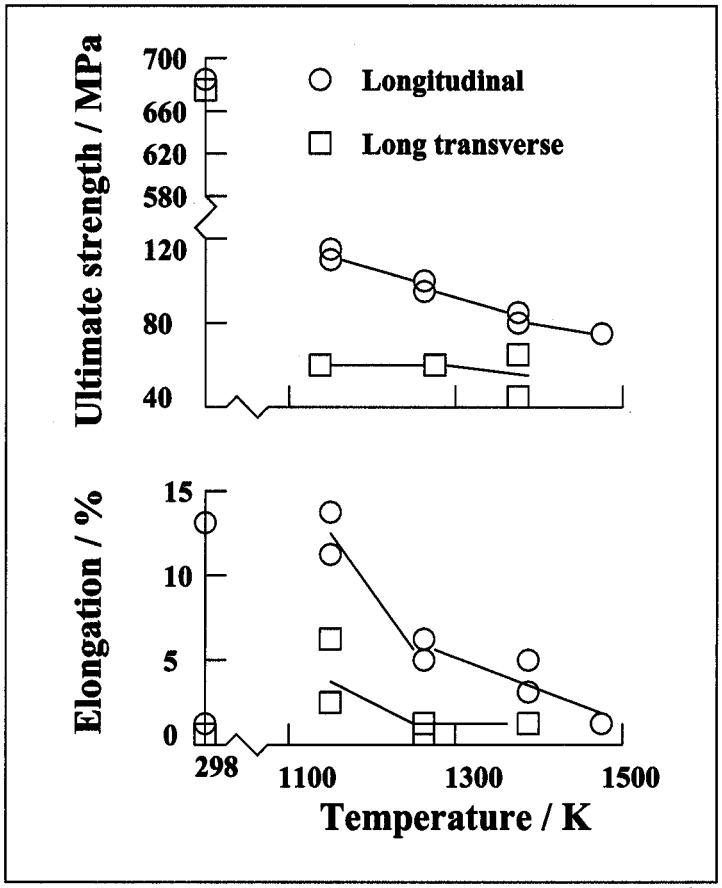

Figure 2.7 : Tensile Properties as a function of temperature for MA956 tested in the longitudinal and long transverse bar direction [Whittenberger, 1981].

and radial directions is shown in Table 2.6. The strength measured along the radial direction was shown to be about 200 to 300 MPa lower than values obtained in the longitudinal direction. Similar observations have been made previously for cold-worked tubes of MA956 and MA957, [Alamo *et al.*, 1990].

The anisotropic behaviour is most probably the consequence of the thermomechanical treatment rather than the mechanical alloying itself. A thin sheet of thoria dispersed nickel-base alloy, TD–NiCr (Ni–20Cr–2ThO_2) produced by internal oxidation of thorium and a standard commercial sheet manufacturing process had been reported to exhibit a similar anisotropic behaviour [Whittenberger, 1976]. For any heat (production batch) of the alloy the tensile properties, stress-rupture strength, and creep strength

Table 2.6 : Tensile strength of 25 % Cold-worked bars of MA957, determined along the radial and the longitudinal directions.

	Radial Direction		Longitudinal Direction	
Test Temperature /°C	0.2 % PS /MPa	UTS /MPa	0.2 % PS /MPa	UTS /MPa
20	893	1035	1360	1388
20	908	1032	1184	1216
450	654	718	1000	1016
450	706	785	965	973

were reported higher for specimens taken parallel to the rolling direction than those of specimens taken normal to the rolling direction. Figure 2.8 shows the stresses necessary to produce 0.1 % creep in 100 h as a function of temperature, direction and sheet thickness. It can be seen that the creep strength of TD–NiCr sheet is greater parallel to the rolling direction than normal to the rolling direction.

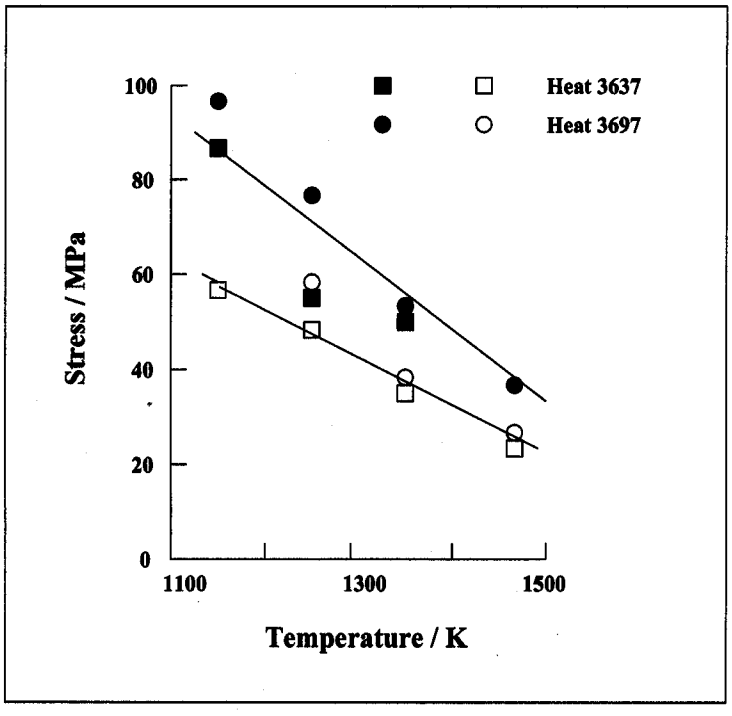

Figure 2.8 : Stress to produce 0.1% creep in 100 h in thin (0.025 cm) TD–NiCr sheet as a function of temperature and direction [Whittenberger, 1976].

However, the compressive strength of mechanically alloyed ODS alloys has been shown to be isotropic. Whittenberger, (1984), conducted a study of the compressive-flow-strength/strain-rate behaviour of MA6000 and observed that the compressive strength was independent of orientation. According to Whittenberger (1984), the inherent strength of ODS alloys is similar in all test directions and the low strength in tension can be traced to the inability of grain boundaries to support large tensile stresses. It follows therefore, that the elongated grain structure with boundaries aligned parallel to the extrusion, direction must have been responsible for the weaker transverse strength.

2.14 Summary

The mechanical alloying technique for the production of oxide dispersion strengthened alloys is a technically viable and potentially promising method for the growing industrial demands for superalloys with better high-temperature capabilities. Mechanically alloyed metals have been developed with a unique coarse columnar grain structure that gives an outstandingly high creep resistance, fine dispersion of inert oxide particles that ensures higher stability at high temperatures, and introduction of reactive elements (Al and Cr) with the attendant higher corrosion resistance and intermediate temperature strength. The alloys have been used in varieties of high temperature industrial applications. However, quite a lot of work is still required in order to understand many of the unusual characteristics of the technique.

CHAPTER THREE

Experimental Techniques

3.1 Materials

The experimental investigations were carried out mainly on MA956, a mechanically alloyed, oxide dispersion strengthened ferritic stainless steel (Table 1.1). The alloy was provided by INCO Alloys, Hereford, U.K. MA956 is produced by charging three primary powders, elemental iron, a pre–alloyed chromium-rich master alloy and yttria, into a water cooled vertical attritor and milled. The resultant powder is consolidated by extrusion at 1000 °C and finally rolled also at 1000 °C. A high–temperature annealing treatment usually at 1300 °C for 30 min is applied to develop the coarse columnar grain structure required to resist creep deformation.

The alloy was supplied as round or rectangular bars and in both the as-extruded and recrystallized conditions. The microstructures in both conditions are shown in Figure 3.1. The as–extruded microstructure consists of elongated grains of less than one micron diameters and grain aspect ratio up to 30 whilst the recrystallized microstructure has coarse grains (10–50 μm) elongated along the extrusion direction with aspect ratio of about 10 [Alamo *et al.*, 1992].

3.2 Stress–Rupture Tests

Samples of MA956 were subjected to various forms of heat–treatments in order to manipulate the grain structure and their stress–rupture properties were tested using facilities at INCO Alloys. Threaded-end specimens with gauge section parallel to the extrusion direction (longitudinal) and perpendicular to the extrusion direction (transverse) were produced. Most of the longitudinal specimens were "standard test pieces", with a gauge diameter and length of 4.51 mm and 23 mm respectively. All of the transverse

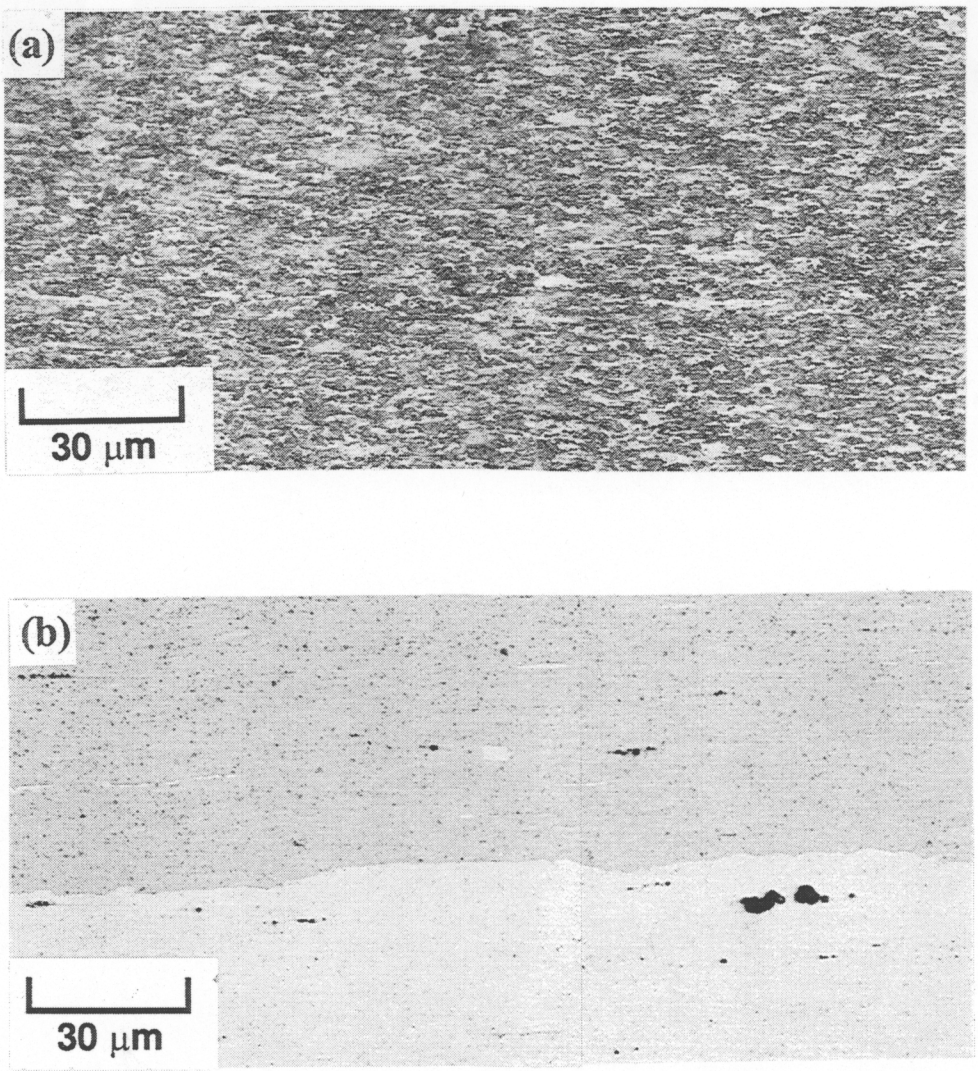

Figure 3.1: Microstructures of MA–ODS ferritic stainless steel, MA956. (a) before recrystallization heat–treatment; (b) after recrystallization heat–treatment (30 min/1300 °C).

specimens and some of the longitudinal specimens were "miniature", with gauge diameter and length of 3 mm and 15 mm respectively, due to the limited size of the bar stock. The stress-rupture tests were conducted in air at 1095 °C in a constant-load tensile creep testing machine under stresses in the range 28 to 79 MPa. The creep ductility was measured using a high temperature extensometry system.

3.3 Hardness Tests

The hardness measurements were made on polished samples using a Vickers pyramid hardness testing machine with an indentation load of 10 kg and a $\frac{2}{3}''$ objective. A minimum of five readings were obtained from each sample and the mean value calculated.

3.4 Tensile Tests

Some room temperature and high temperature tensile tests were conducted on the recrystallized and unrecrystallized MA956. The room temperature tensile samples were machined from a rectangular bar of MA956 in the as-extruded condition, both along the working direction and normal to the working direction. The samples used in the investigation of the temperature dependence of the tensile properties of the alloy in the as-extruded condition were machined from a different batch of the material, in the form of a round bar of 10 mm diameter. Only logitudinal samples could be obtained in that case. The specimens for high temperature testing were slightly bigger than those for ambient tests because different accessories are required when the testing machine is fitted with a heating furnace (Figure 3.2).

The room temperature tests were carried out on a "Schenck Trebel", universal screw–driven test machine with a maximum loading capacity of 50 kN. The high temperature tests were on a "MAND" universal testing machine which is similar to the Schenck Trebel machine but with a design which makes it suitable for use with a furnace assembly.

3.5 Optical Microscopy

Samples were prepared for optical metallography by hot mounting in conductive bakelite powder, followed by grinding on SiC paper to 1200 grit and polishing with 1 μm cloth coated with diamond paste. They were etched using a reagent which is made up of 2 g CuCl2, 40 ml HCl and, 40 to 80 ml ethanol. Optical micrographs were taken with an Axiotech microscope with a Yashica camera attached.

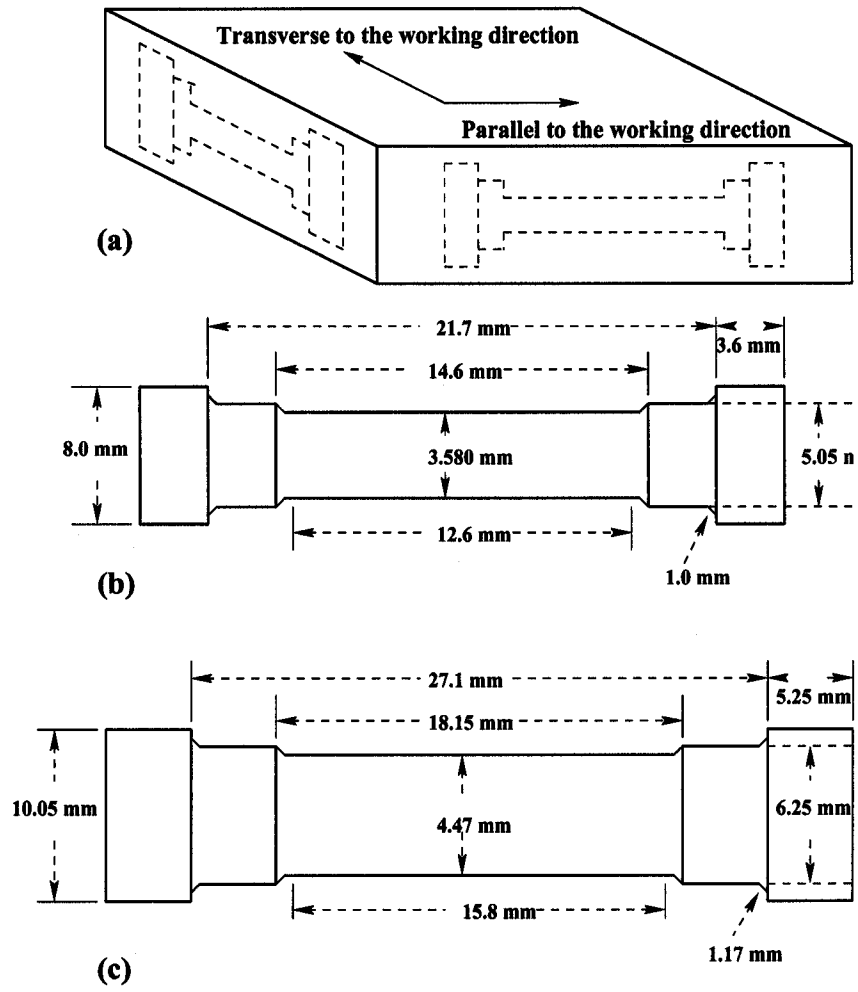

Figure 3.2 : Specimens used for the tensile tests, (a) rectangular bar showing sample orientations, (b) room temperature test specimen, and (c) high temperature test specimen.

3.6 Scanning Electron Microscopy (SEM)

A Jeol–820 scanning electron microscope was used to examine some metallographic specimens and fracture surfaces. Fractured Samples were mounted onto stubs using an Araldite adhesive mixed with graphite powder to prevent charging during imaging. An FP4 film was used on the attached camera.

3.7 Energy Dispersive X–ray (EDX) Microanalysis

Chemical microanalysis was carried out using an EDX system on a Camscan S4 scanning electron microscope. ZAF4, is a suite of computer programs which permits the calibration and routine quanti-

tative electron microprobe analysis. The X–ray emissions were interpreted using these programs. The microscope was operated at 20 kV with the stage tilted at 45°. The specimen is inserted in the EDX holder with the Co standard on the rim. The system is calibrated by the reference spectrum collected from the analysis of the Co standard and the quality of the subsequent analysis depends on the accuracy of the calibration.

3.8 Transmission Electron Microscopy

Carbon extraction replicas were prepared to oxide particles in a Phillips 400T transmission electron microscope operated at 120 kV.

Single–stage carbon extraction replicas were prepared using the method described by Smith and Nutting (1956) from optical microscopy samples using a light etch (2 g CuCl2, 40 ml HCl and, 40 to 80 ml ethanol). A carbon coating of 200-300 Å(colour blue–brown) was deposited in a vacuum of 10^{-5} torr on to the etched specimens. The carbon film was scored using a sharp blade to enable the removal of several small sections covering the whole area of the sample. The film was then removed by electrolytic etching in a solution containing 5 % hydrochloric acid in methanol at +1.5 V. The film was washed in industrial methylated spirits and floated off in distilled water and then collected on 200 square mesh copper grids for examination in the TEM.